Evidence for magmatic hydrothermal mineralisation at Kanmantoo Copper deposit, South Australia.

Thesis submitted in accordance with the requirements of the University of Adelaide for an Honours Degree in Geology

Nick Lyons

November 2012

HILLGROVE RESOURCES

THE UNIVERSITY of ADELAIDE

ABSTRACT

The Kanmantoo Cu-Au deposit is located 55km east of Adelaide, on the eastern edge of the Mt Lofty Ranges, South Australia. It is of Delamerian age and is hosted in the Tapanappa series of the Kanmantoo Group, a pelitic turbidite sequence metamorphosed to amphibolites facies. Models for mineralisation vary from sedimentary exhalative system to epigenetic mineralisation. Despite recent work, the structural evolution of the deposit is largely unknown and this allows for the absence of a definitive model for mineralisation. Detailed face mapping of the 1190RL bench in conjunction with handheld X-Ray Fluorescence Niton gun was adopted to further investigate the relationship between key structural features and element distribution. Micro analysis by petrographic studies, Edax element maps and $\delta^{34}S$ isotope analysis was completed to gain understanding into fluid-rock relationships and origin of mineralising fluids. The findings of this study strongly suggest timing of copper mineralisation was associated with the first phase of orogenic extension at 490 ± 3 Ma. The extensional reactivation of compressional D3 shear zones, along with the injection of partially oxidised igneous derived fluids interacting with Fe-rich sediments, allows for the formation of the Kanmantoo magmatic hydrothermal deposit. Sulphur isotope results, and the mapping of magnetite-pyrite-chalcopyrite bearing K-feldspar veins are a very strong evidence of an igneous influence. Cu precipitation is as a result of a cooling oxidised magmatic hydrothermal fluids reacting with Fe in metasediments, and partially interacting with a reducing environment, rather than being directly associated with Fe rich metasomatism. Broad unmineralised zones of chlorite alteration suggest circulation of magmatic hydrothermal fluid with copper mineralisation preferentially precipitating in veins within and adjacent to reactivated D3 shears and D3 antiformal zones.

KEYWORDS

Magmatic hydrothermal, post-orogenic extension, K-feldspar veins, copper – gold.

Table of Contents

LIST OF FIGURES AND TABLES

INTRODUCTION

The structural controls and relative timing of mineralisation at the Kanmantoo Cu-Au mine are poorly understood. Early studies of drill core from the Kanmantoo mine (Lindqvist 1969) led to suggestions that copper mineralisation was syn-sedimentary and thus it was considered to be hosted within the limbs of a regional syncline. This was later supported by Verwoerd and Cleghorn (1975). Marshall and Spry (2000) again argued that the overall evidence gathered from the Kanmantoo deposit suggested a pre-tectonic, sedimentary exhalative mineralisation system.

New thinking on the structural controls and style of mineralisation was developed after Oliver et al. (1998) completed a study investigating the bulk chemistry and oxygen isotopes from the collection of rock samples from within the Kanmantoo mine area. The result of this study determined geochemical indicators that may tie alteration to specific processes, which lead to a suggestion that mineralisation was derived from fluid derived from granite in an event that occurred after early orogenic folding. This relative timing of mineralisation was supported by Wilson (2009) after monazite microprobe Th-U-Pb dating of a sample of recent drill core in the main zone suggested an age of 492 ± 9 Ma for mineralisation. This post dates peak metamorphism and contractional deformation (Foden et al., 2006). Focke (2010) produced similar results of 469 ± 17 Ma and 498 ±16 Ma after dating satellite deposits and both authors suggest that these dates, along with structural observations of drill core and regional mapping indicate that mineralisation is in association with late phase, post-orogenic magmatism.

Most recently, Arbon (2011) has suggested that there are several alteration events, namely two distinct chlorite alteration events each associated with different mineralisation in each event. Recent face mapping by current mine geologists at the Kanmantoo mine further supports the cross cutting nature of mineralisation however the specific relationships between mineralisation and Delamerian structures are poorly constrained.

With the recent exposure of fresh surfaces and structures from the re-opening of the Kanmantoo pit by Hillgrove Resources in November 2010, new insights to these problems can be gained. This can be done by identifying vein and alteration assemblages and linking them to mappable structures that can be placed within a regional context and their timing relationship to the Delamerian Orogeny.

In this paper I present detailed face mapping of recently exposed and unmapped surfaces, coupled with handheld XRF geochemical mapping that helps to demonstrate the link between structures and mineralising fluids. This will test the hypothesis that copper – gold mineralisation is related to late Delamerian magmatism. This has allowed constraints to be determined on the relative timing of veins and alteration with respect to structural events associated with the Delamerian Orogeny. Further investigation by thin section, ion microprobe and sulphur isotope work helps evaluate the nature of mineralising fluids, along with understanding the permeability of the host rock during mineralisation at the Kanmantoo copper deposit. This will contribute to the model of mineralising systems in the Adelaide Fold Belt (AFB) which will help develop a predictive model for mining methods, near mine exploration and for regional controls on mineralisation.

GEOLOGICAL SETTING

Background Geology

The Kanmantoo Cu Au deposit is located in the Kanmantoo Group, on the south-eastern edge of the Adelaide Fold Belt (Oliver, 1998)(figure 1). The 7-8km thick Kanmantoo group is identified as the youngest part of the Neoproterozoic to Cambrian Adelaide Geosyncline (Haines, 2001). The Kanmantoo Group consists of metamorphosed clastic turbidites with occasional psammitic beds up to 5 metres in thickness (Haines, 2001). The Kanmantoo Group unconformably overlies the Neoproterozoic Normanville Group. This unconformity is suggested to represent a dramatic change in tectonic regime from a late Neoproterozoic passive continental margin to an early to mid-Cambrian convergent subduction margin (Jenkins and Sandiford 1992; Foden et al., 1999).

The sedimentation of the Kanmantoo group occurred in a rapid rifting phase, allowing fast deposition rates. The source of the sediments has been suggested by Foden et al. (1999) to be from the Ross Orogen to the south which was also supported by paleo-current analysis conducted by Haines (2001).

The minimum age of the Kanmantoo Group deposition is defined by the Rathjen Gneiss, an intrusion which occurred during the first stage of syn-tectonic magmatism, (Foden *et al.* 1999). Foden et al. (1999) report a U – Pb zircon age of 514 ± 5 Ma for this gneiss which suggests very rapid deposition of the Kanmantoo Group over a period of approximately 10 Ma or less (Flottmann *et al.* 1998, Jago *et al.* 2003).

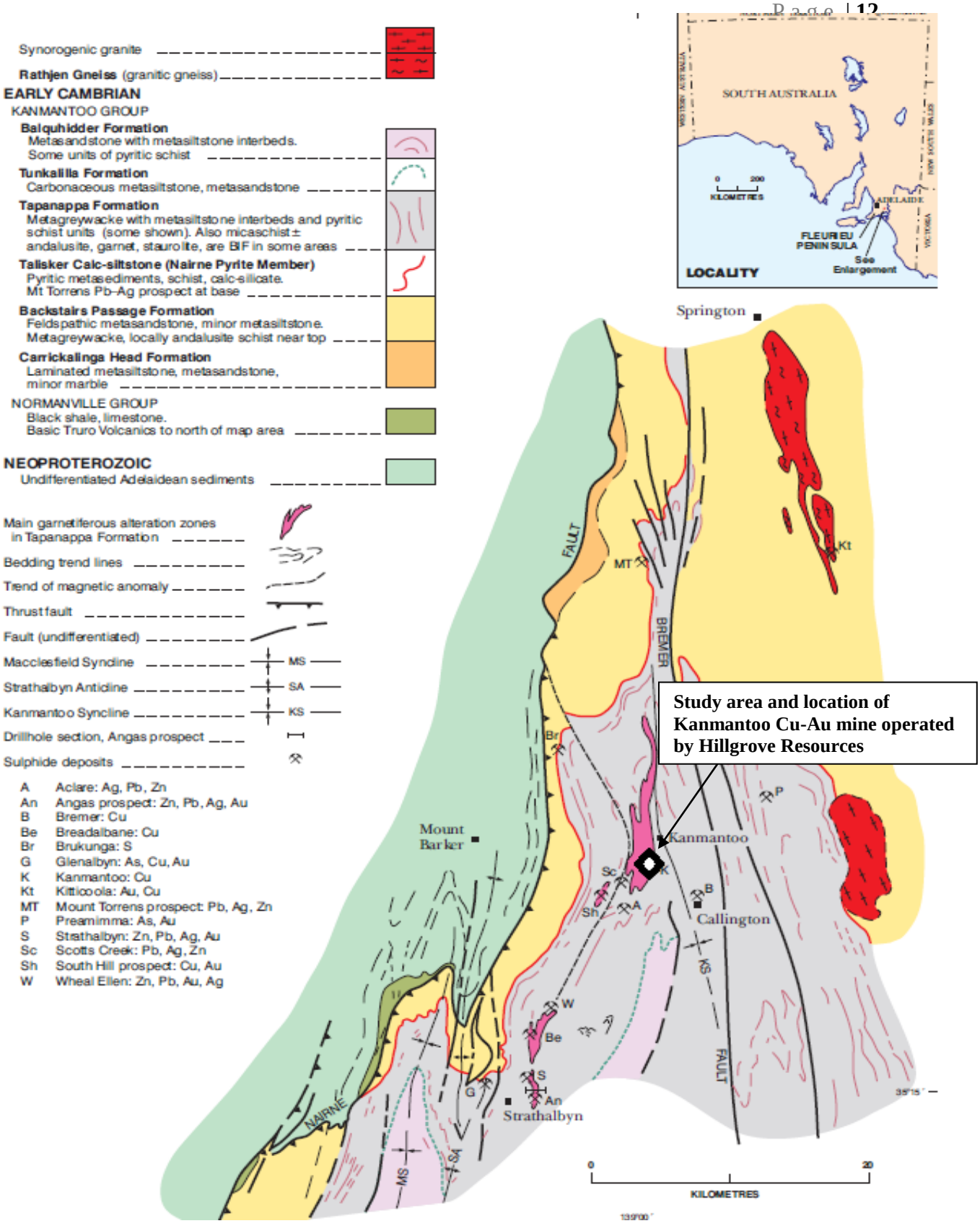

Figure 1: Adapted from Toteff (1999) showing location of the Kanmantoo Copper mine and its relationship to the regional geology of the Kanmantoo Trough. Regional structural features such as Kanmantoo and Monarto Synclines are shown in conjunction regional major faults, lithological units and known intrusives of the region. Known mineral deposits have been indicated, along with the Tapanappa formation, which host many of these deposits.

The Kanmantoo Cu-Au deposit occurs within the Paringa Andalusite Member of the Tapanappa Formation, (figure 1) (Mancktelow, 1979; Spry et al., 1988; Both, 1990, Gum, 1998). The Tapanappa Formation is a thick sequence of silty sands which conformably overlies the Talisker Calc-siltstone Formation. The Tapanappa Formation consists of thin siltstone and mudstone units, which are often rich in pyrite and pyrrhotite and anomalous in base metals (Gum et al., 1994). The Tapanappa Formation is known to contain a number of other syngenetic and epigenetic base-metal deposits. (Parker 1986; Both 1990; Belperio *et al.* 1998). It is interpreted to represent the onset of a period transgressive sedimentation with turbiditic sediments deposited in a rifting and rapidly subsiding continental margin of submarine shelf sediments (Schiller, 2000).

The Delamerian Orogeny was initiated with an abrupt cessation of sedimentation in the Kanmantoo trough (Parker 1986, Jago *et al.* 2003, Foden *et al.* 2006). This was due to major compressional tectonics associated with the subduction along the edge of Gondwana (Flottmann *et al.* 1998, Foden *et al.* 2006) . This orogenic event is characterised by several stages of deformation and metamorphism, most commonly recognised as deformation events 1-3 (D1, D2 and D3) (Jenkins & Sandiford 1992, Flottmann *et al.* 1998, Jago *et al.* 2003). D1 has been recognised as tight to isoclinal, upright to inclined folds generally following the curvature of the belt, and is associated with a fabric (S1), which is most intense within D1 thrusts and shear zones (Jenkins & Sandiford 1992, Flottmann *et al.* 1998, Jago *et al.* 2003). D2 produced tight to isoclinal folds, common only in high strain zones with S2 axial planar fabrics expressed as crenulations of S1 or penetrative schistosities in higher grade rocks representing peak metamorphic conditions. D2 also produced a series of reverse and

strike slip faults (Jenkins & Sandiford 1992, Flottmann *et al.* 1998, Jago *et al.* 2003). D3 is suggested to have produced local folds and shear zones commonly with west to northwest-trending axes and generally easterly dipping axial planes (Jenkins & Sandiford 1992, Flottmann *et al.* 1998, Jago *et al.* 2003). The overall result of this deformation developed a series thrust faults and partially overturned westward vergent folds (Foden *et al.* 2006).

Metamorphism during the Delamerian Orogeny is of high temperature, low pressure facies ranging from chlorite to sillimanite grades (Sandiford *et al.* 1990). Metamorphism is associated with the convergent D1-D3 events of the Delamerian Orogeny, outlined above. Andalusite and sillimanite metapelites of the Mt Lofty Ranges indicate peak conditions of 550-600°C, and pressures of 300-500 MPa (Sandiford *et al.* 1995). Concentric zoning of isograds are spatially associated with north-northwest trending syn-metamorphic intrusives. These intrusive rocks facilitated advective heat to initiate metamorphism (Sandiford *et al.* 1995).

Several stages of magmatism accompany the Delamerian Orogeny. Early magmatism firstly involves basalts and dolerites related to the extensional formation of the basin (Floettmann *et al.* 1998, Flöttmann *et al.* 1998). A transition to I-type and S-types syn-orogenic granites occurred (Foden *et al.* 1990), which was followed by bimodal magmatism with A-type affinities that cluster towards the mantle end-member (Foden *et al.* 2002c). This latest phase of magmatism has been recognised to be associated with the transition from convergent, subduction-related, tectonics to extension, reflecting orogenic collapse and exhumation related to a possible slab-rollback (Foden *et al.* 2002c). This tectonic event is also marked by a series of NNW-SSE striking

mafic and felsic dykes that are suggested to accompany this post-orogenic collapse (Foden *et al.* 2002c).

Metamorphism at the Kanmantoo deposit

Mineralisation at the Kanmantoo deposit occurs within a 6km wide iron-rich pelitic schist dominated by garnet + andalusite + biotite + quartz, with local occurrences of staurolite ± chlorite (Parker 1986, Oliver *et al.* 1998, Abbot 2005). This mineralogy differs from the metamorphic assemblages in the surrounding Tapanappa Formation in that muscovite and cordierite is rarely present, whereas andalusite, staurolite, chlorite and magnetite are common. This suggests a general Fe enrichment and a reduction of Na and Ca proximal to the mineralisation (Oliver *et al.* 1998). Metamorphic phase relations during the Delamerian Orogeny are consistent with metamorphism at high temperature low pressure conditions with peak temperatures at approximately 550^{o} C in the sillimanite zone and 450^{o} C in the biotite zone (Dymoke & Sandiford 1992, Oliver *et al.* 1998).

Metamorphism of rocks within the mine sequence differs to those surrounding the deposit with host rocks showing less microstructures (Oliver *et al.* 1998, Schiller 2000). Geology surrounding the Kanmantoo deposit reflects the complex deformation history, whereas locally, it is thought that peak metamorphic conditions have proceeded longer than the D3 deformation and has eliminated earlier D1 and D2 structures (Oliver *et al.* 1998). A weak crenulation fabric is present that is loosely similar in direction to the surrounding, much more pronounced, S3 fabric (Oliver *et al.* 1998).

MINERALISATION AT THE KANMANTOO DEPOSIT

Mineralisation at the Kanmantoo copper deposit occurs predominantly as chalcopyrite (Seccombe *et al.* 1985, Parker 1986, Oliver *et al.* 1998, Schiller 2000, Abbot 2005). Pyrrhotite, magnetite, pyrite, covellite, chalcocite and sphalerite are also present in variable levels throughout the vein regime (Seccombe *et al.* 1985, Parker 1986, Oliver *et al.* 1998, Schiller 2000, Abbot 2005). Other minerals such as marcasite, galena, silver, molybdenite, wolframite and native bismuth or bismuthinite occur within the Kanmantoo deposit however it is not known if these minerals are associated with Cu-Au mineralisation (Parker 1986, Schiller 2000, Abbot 2005).

The copper mineralisation is, predominately in pipe-like podiform lenses dominated by chalcopyrite. This mineralisation is believed to be predominantly within S3-parallel quartz veins discordant to relict bedding. This bedding has undergone thickening due to folding (Oliver *et al.* 1998, Abbot 2005). Oliver *et al* (1998) has suggested mineralisation may have been due to Fe-rich fluid metasomatism. Evidence for this is found in the decussate texture of biotite, garnet and staurolite in association with mineralisation, possibly suggesting low strain rates or accelerated fluid assisted diffusion (Oliver *et al.* 1998).

Interpretations of the origin of mineralisation within the Kanmantoo Group differ (Windsor *et al,* 1999). Seccombe *et al.* (1985) suggested that many of the deposits in the Kanmantoo Group were formed by hydrothermal fluids expelled from depths of 3–4 km in a sedimentary basin. Parker (1986) identified the importance of structural features in localising ore fluids and related mineralisation sites to the intersection of northwest-trending fractures and pyritic horizons. More recently Wilson (2009) and

Arbon (2011) have suggested mineralisation is associated with late stage orogenic granites and the localisation of magmatic hydrothermal fluids.

The structural complexity of the Kanmantoo Group, in particular thrust faulting, and a lack of regional marker beds, has resulted in the absence of a detailed structural understanding of the Kanmantoo Group (Seccombe *et al.* 1985, Parker 1986, Schiller 2000, Haines, 2001). This in turn contributes to the uncertainty regarding the structural evolution of the Delamerian Orogeny and its relationship to other orogens on the Palaeo - Pacific margin (Flottmann *et al.* 1994). This study uses the recently exposed faces of the Kanmantoo mine to complete an investigation will linking mineralisation, local and regional alteration and key structural features. This leads to understanding the timing of the deformation events of the Delamerian Orogeny and in turn how these deformation events control mineralisation and alteration at the Kanmantoo Cu-Au mine.

METHODS

Field work.

Field work was undertaken along 170 metres of the 1190 RL bench in the Spitfire Pit of the Kanmantoo copper mine (figure 2 and figure 3). Field work was conducted in several stages to provide a structural analysis of the setting of the Kanmantoo copper deposit, focusing on the structural controls of mineralisation and alteration present. Analysis included collecting general observations of macro and micro structures, structural mapping, vein paragenesis and the relationships of these structural features to geochemical analysis.

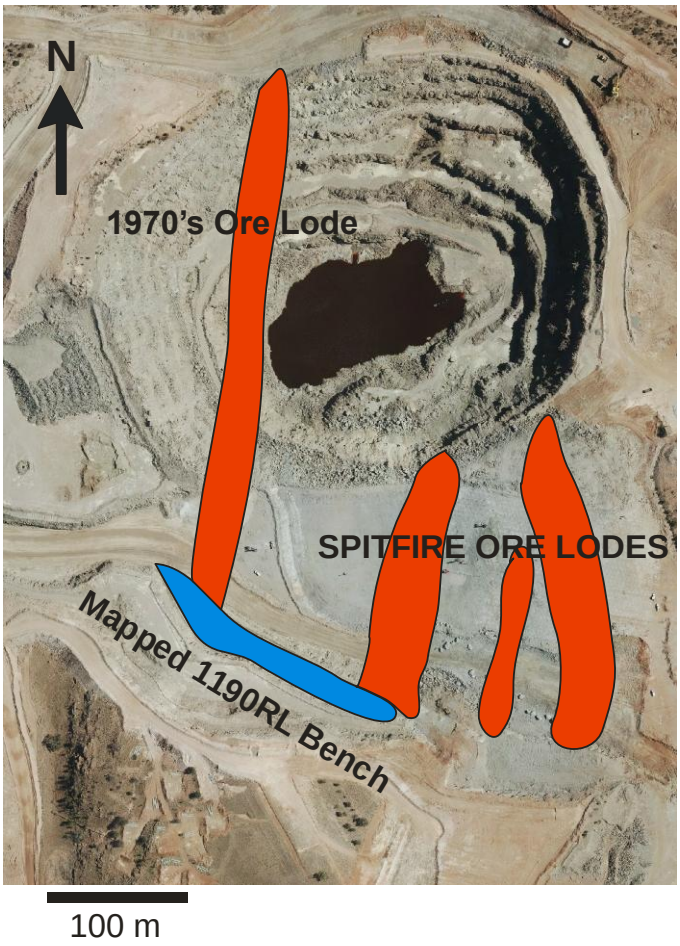

Figure 2: Aerial photograph of the 170m 1190RL bench mapped in this study (blue), shown against the 1970's ore lode and current Spitfire pit ore lodes. Spitfire pit lodes are indicated from Hillgrove Resources modelling (2012).

The mapping focused on lithology and alteration as well as all structural features such as foliation, bedding, cleavage sets, faults, folds that were present. The mapping took special interest in S-C fabric and any veining, specifically quartz, sulphide or other, which was present along with any apparent cross cutting relationships to determine the relative timing of veining with respect to all other fabrics present along with any alteration that may accompany the veining.

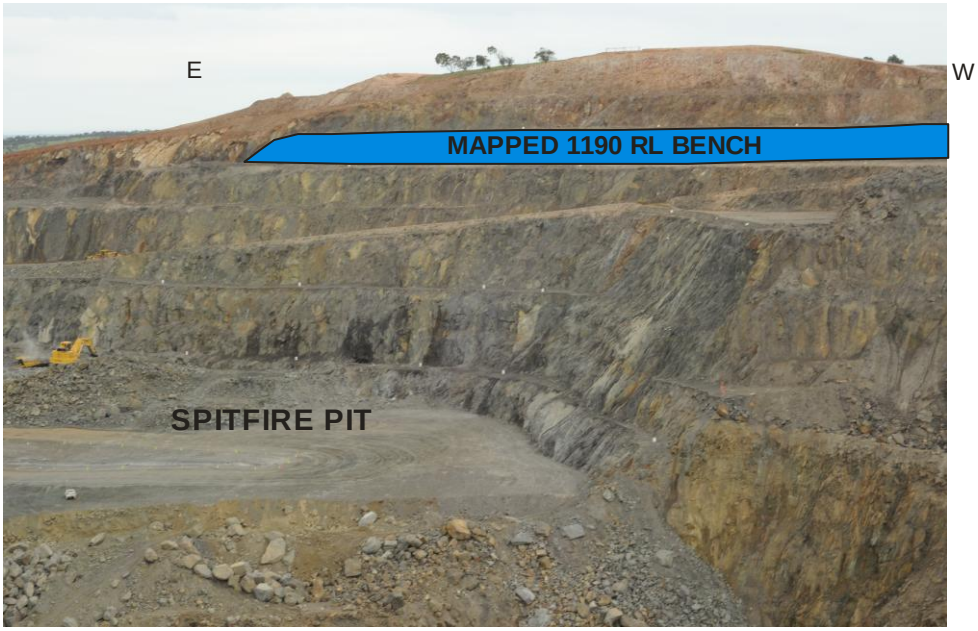

Figure 3 : Looking south towards the 170m mapped 1190RL face, showing its relationship to the current Spitfire pit.

This involved measuring the orientation of veins that were discovered during mapping along with recording their specific lithology, size and any deformation present. A vein younging table was then completed (Potts et. al, 1999) to determine the order and timing of the veins present. This was completed by analysing the cross cutting relationships of the veins to each other to determine the order of vein paragenesis. Geochemical analysis of the mapped 1190 RL bench was then undertaken by XRF handheld Niton. This was done in 2 stages:

1. BULK GEOCHEMISTRY

Portable XRF measurements were taken using a handheld Niton XRF device, in two parallel profiles across the entire mapped face. The lower ‘A’ profile was on average 1 metre above the base of the bench, while the ‘B’ profile was 30cm higher. Analyses were taken at 40cm intervals for a total of 896 analyses. The handheld Niton XRF has a 0.2cm field of view. The sample time was 1 minute, running 4 filters for 15 seconds each (appendix B). This reading length has been advised to be appropriate by the Niton handheld XRF manual as sufficient for each filter as errors for each element are sufficiently low after this reading time. Calibrations and standards can be seen in appendix B . This approach was undertaken to enable a rapid acquisition of large datasets in which broad trends can be identified for closer, more precise analysis.

2. LOCALISED GEOCHEMISTRY

After analysis of bulk geochemistry against face mapping, 4 areas that showed significant mineralisation or structural significance to mineralisation were selected for closer geochemical analysis. These areas are 1 square metre, and involved XRF Niton analysis on a 10 x 10 cm grid. This closer grid spacing was in order to obtain better resolution and accuracy with the Niton handheld XRF and give a more detailed geochemical analysis. Standards were again run in a similar manner outlined in the bulk geochemistry sections above. The grids were photographed, with the geochemical results overlain to allow analysis of micro structure and their relationship to element distribution.

Micro – analysis

THIN SECTION

From results gathered during field mapping and XRF Niton geochemical sampling samples representing different vein generations, alterations and geochemical trends were taken for thin section to allow micro analysis. Polished thin sections were prepared by Pontifex, and micro-structural analysis was conducted on a Nikon petrographic microscope.

EDAX ELEMENT MAPPING

To further investigate mineral chemistry of the ore minerals, chlorite alterations and gangue phases, element maps were taken on the XL - 40 instrument with wavelength-dispersive spectrometers at Adelaide Microscopy. 30 µm polished carbon coated thin sections made by Pontifex were used for this analysis. A sulphide package was used containing 16 elements for which the weight percentages were calculated. This package was used on chalcopyrite, pyrrhotite, pyrite and sphalerite. Standards were utilised for each individual element from Adelaide Microscopy. A silicates package containing 18 calibrated element oxides to be measured was used for garnet, chlorite, biotite, as well as magnetite.

SULPHUR ISOTOPE ANALYSIS (SIMS)

The CAMECA IMS 1280 high resolution, multi-collector ion microprobe (CAMECA 2012), located at the Centre for Microscopy, Characterisation & Analysis (CMCA) at The University of Western Australia, was used to perform sulphur isotope analysis ($^{34}S/^{33}S$) from chalcopyrite grains hosted within copper bearing quartz veins and copper bearing K-feldspar veins. Variations in sulphur isotopes were used to identify

the possible source of the sulphur, and to determine ore genesis in relation to sulphur signatures gained from vein sets of differing orientations.

RESULTS

Face mapping

Primary Lithology

Several differing lithologies were mapped on the 1190RL bench (figure 4).

GABS – Host rock. A garnet andalusite biotite schist. Andalusite grains are fine to medium, and the overall porphyroblasts are ~0.5cm but may be up to 2 cm. The rock is schistose in texture often with elongate andalusite parallel to foliation. Fine garnet is present and some areas are very rich in biotite. There is a distinct lack of muscovite present in this unit. This lithology is commonly seen in unaltered and unmineralised areas of the Kanmantoo mine.

BGCS - Biotite garnet chlorite schist ± staurolite. Chloritisation of this schist is seen to vary from highly chloritised schist, commonly around veins and other structures, to moderately chloritised with remnant andalusite present. Intense and coarse grained garnet selvages are commonly present either parallel to or cross cutting foliation.

GBP - Garnet biotite muscovite pelite ± sillimanite, pyrrhotite. This rock type is commonly found in association with shear zones. Units are 1-2 metres thick and show overprinting and destruction of andalusite in fabrics. Small garnet growth is present, along with minor pyrite and pyrrhotite along fabric of the rock.

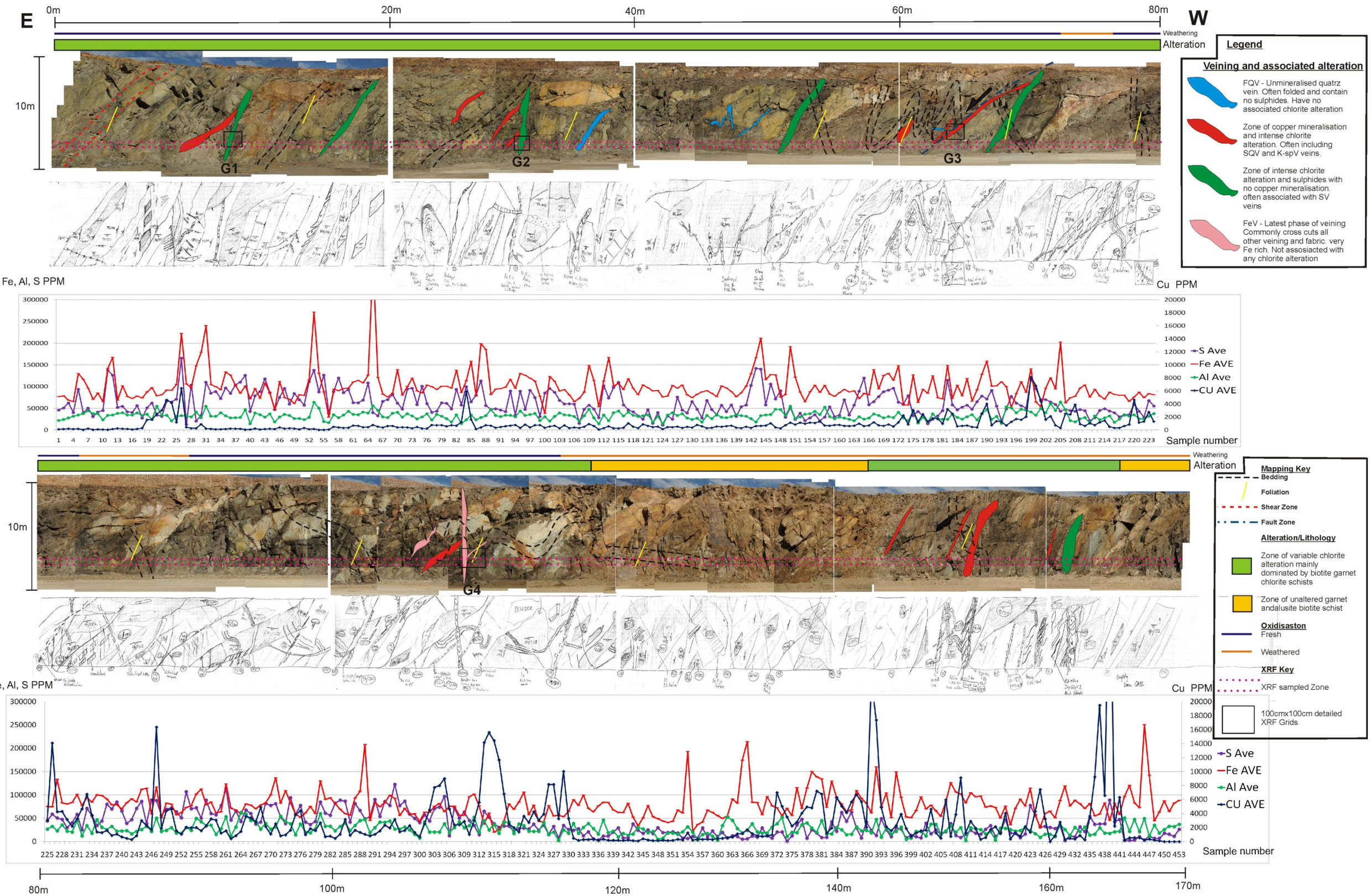

Figure 4 : Mapped 170m of 1190 RL bench with Bulk XRF sampling of S, Fe, Al (left axis) and Cu (right Axis). Folding, faulting, veining, alteration and oxidation are overlain over stitched photographs of the mapped face, with mapping interpretation shown underneath. Bulk XRF sampled zone are shown as the average of the A and B samples. Handheld XRF results displayed are Fe, Al and S PPM (left Axis) and Cu PPM (right axis). Mineralised K-spV and SQV veining are shown to cross cut folding and also commonly cross cut foliation. Mineralised K-spV, SQV and unmineralised SV veins are all seen to be spatially related to chlorite alteration are seen in association with chlorite alteration. Fev veins are seen to cross cut all veining and fabrics. Broadly, chlorite alteration is consistent with elevated levels of S, while Cu mineralisation is locally controlled by K-spV and SQV veins and the normal fault (60-64m) and parasitic fold hinges in the vicinity of this fault. Fe distribution shows occasional increased levels around some veins and chloritised zones, however background levels are consistently between 50000-100000 ppm (5-10%) throughout both unaltered and altered zones.

BEDDING

Bedding is seen to be tightly folded in areas (figure 4), and is often truncated by shear zones and faults. These beds have been identified by the presence of very fine siliceous layers present in otherwise very homogeneous, highly altered and overprinted textures. Bedding was also determined by fine pelitic and psammitic distinctions within the GABS unit. Younging directions were not established largely due to the overprinting present in the mapped area.

Ductile deformation

FOLDING

Folding is present in between metres 50-60m and 105-120m on the 1190RL bench (figure 4). Several fold hinges were mapped are measured to be slightly south plunging with an 18/210 (dip/dip direction) orientation. Tight folding is seen to be associated with a fault zone between metres 60-65 on the mapped face (figure 4). The overall geometry of the folding is measured to be a series of parasitic folds on the eastern limb of a regional synform closing to the west. This is consistent with previous mapping completed by current mine geologists and throughout the early years of the mine in the 1970's. The axial surface is near vertical and parallel to the steeply east dipping foliation and has a mean of 75/100. Foliation cross-cuts bedding in several places and this relationship is shown in figure 4 above.

SHEARING

One shear zone was mapped in the 1190 RL bench and is located between metres 0 and 3 (figure 4). This shear cross cuts foliation and overprints earlier GABS fabrics. High strain seen in mineral assemblages associated with this zone and can be seen in thin section SI-0-5 (figure 8).

Brittle deformation

FAULTING

Only one fault was mapped 1190RL bench. A normal fault was mapped at 62 metres, and is highlighted by Grid 3. This fault has and orientation of 56/110, and clearly cross cuts and displaces earlier fabrics (figure 4 and figure7 – grid 3). Copper bearing K-feldspar veins infill the fault surface and are common around the fault zone. Displacement and kinematics were determined by the normally offset bedding (figure 4), and the timing of this fault was determined as it cross cuts all previous ductile deformation events.

Veins and associated alterations.

VEINING

5 different vein sets and lithologies were observed during mapping on the 1190RL bench (Table1). Mineralisation is commonly present with SQV and K-spV veins. Only minor traces of Au and Bi were detected and were found in association with SV veins and associated alterations. FQV and FeV veins were found to be barren from any mineralisation. The Potts and Reddy (1999) method for systematic assessment of relative deformation was used to analyse the cross-cutting relationships observed in the five differing vein lithologies. Table 2 is a younging table used to determine the relative timing of these veins across the 1190RL bench. Results determined order of vein formation were Oldest ; FQV, through to K-spV, SQV, SV with FeV clearly being the youngest veining event, as these veins cross cut all other veins and fabrics.

Table 1 : Vein lithology table of the 5 differing vein types mapped across the 1190RL bench. Colour coding is in conjunction with face mapping (figure 4), where spatial distribution and relationships to alteration and bedding can be seen. Mineralisation is commonly present with SQV and K-spV veins. Only minor traces of Au and Bi were detected and were found in association with SV veins and associated alterations. FQV and FeV veins were found to be barren from any mineralisation.

Vein	Orientation	description	Picture
Folded quartz veins **(FQV)**	fold hinges often show an axial plane of 81/099, and have a hinge plunging 10-15 degrees to the south	Folded quartz veins with no copper mineralisiation present. Commoly show Fe staining and are 5 to 15 centimetres in diameter.	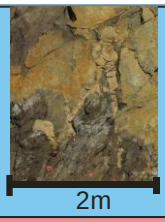
Sulphide bearing quartz veins **(SQV)**	commonly orientated 70/099 and are often slightly boudinaged.	Sulphides include chalcopyrite, pyrrhotite and pyrite. Veins are 5 cm – 120 cm in diameter. Commonly associated with staurolite growth at contact with the vein and the surrounding country rock.	
Copper bearing K-feldspar veins. **(K-spV)**	Commoly orientated 67/100	Veins contain k-feldspar, quarts, biottie, muscovite and sulphides, are 10-30 centimetres in diameter. Staurolite growth is present at contact of vein and country rock.	
Sulphide veins. **(SV)**	Orientation 85/110, 72/094	Pyritic veins 5 mm to 10cm in diameter. Sulphides include Pyrite, Chalcopyrite, Pyrrhotite.	
Ferruginous quartz veins **(FeV)**	Commonly orientated 85/115, 83/173.	Vary from 5 cm – 30 cm in diameter. Highly Fe rich veins that cross cut all other fabrics. Little deformation present around veins.	

Table 2: Table 3: A Potts and Reddy (1999) style vein younging chart of the 5 differing vein lithologies from the mapped 1190 RL bench as outlined in table 1. Cross cutting relationships of veins were used to determine the oldest (FQV)

		Youngest				Oldest
		FeV	SV	SQV	K-spV	FQV
Youngest	FeV	0	–	–	–	–
	SV	↑	0	–	–	–
	SQV	↑	↑	0	–	–
	K-spV	↑	↑	↑	0	–
Oldest	FQV	↑	↑	↑	↑	0

↑ - arrow points to younger veining event

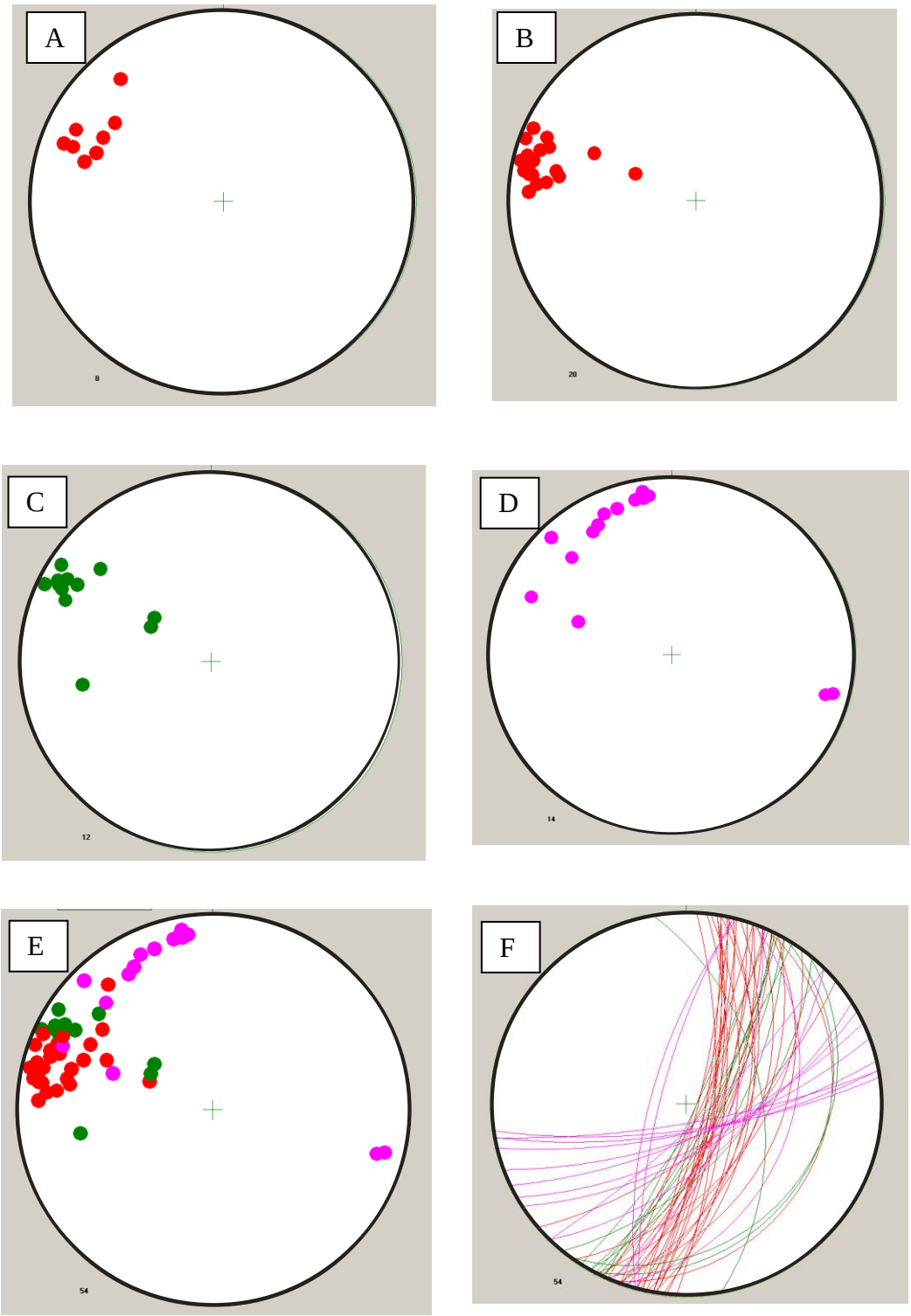

Figure 5 : Stereonets of pole points (A-E) of vein lithologies and planes of all mapped veins (F). Colours are in conjunction with Table 1. A: K-spV veins with a mean orientation of 67/105. B: SQV veins with a mean orientation of 79/099. C: SV veins with a mean orientation of 84/115. D: FeV veins with a mean orientation of 83/173 E: pole points of all veins. F: Planes of all veins highlighting the rotation in stress regime from initial E dipping SQV and K-spV veins to youngest S dipping FeV veins.

ALTERATION

Varying intensities of chlorite alteration were mapped across the 1190RL bench (Figure 4). This chlorite alteration was seen to be in two phases. One phase of alteration formed sheets orientated approximately 72/099 and commonly associated with SQV veins and K-spV veins (CHL1).This was cross cut by a later phase of chlorite alteration of variable width and seen to be associated with discrete shear zones and sulphide veins (SV) commonly orientated approximately 84/115 (CHL2). These zones have been highlighted in the face mapping in figure 4

Bulk XRF analysis suggested that chemically these zones differ, and this was the focus of the close spaced handheld XRF Grids (figure 6). Details of these close spaced grids can be seen in table 3.

CHL1, seen in grid 3 (figure 6), clearly overprints andalusite but also commonly shows increased garnet growth and selvages (table 3). This garnet growth cross cuts foliation and forms melanosomes of garnet in areas proximal to copper bearing quartz and K-feldspar veins. CHL1 alteration is associated with copper mineralisation hosted in vein form (grid 3) and also disseminated in some areas, such as grid 4 (figure 6 and table 3). Contacts with host rock are gradual and show grading from host rock to altered rock on a metre scale.

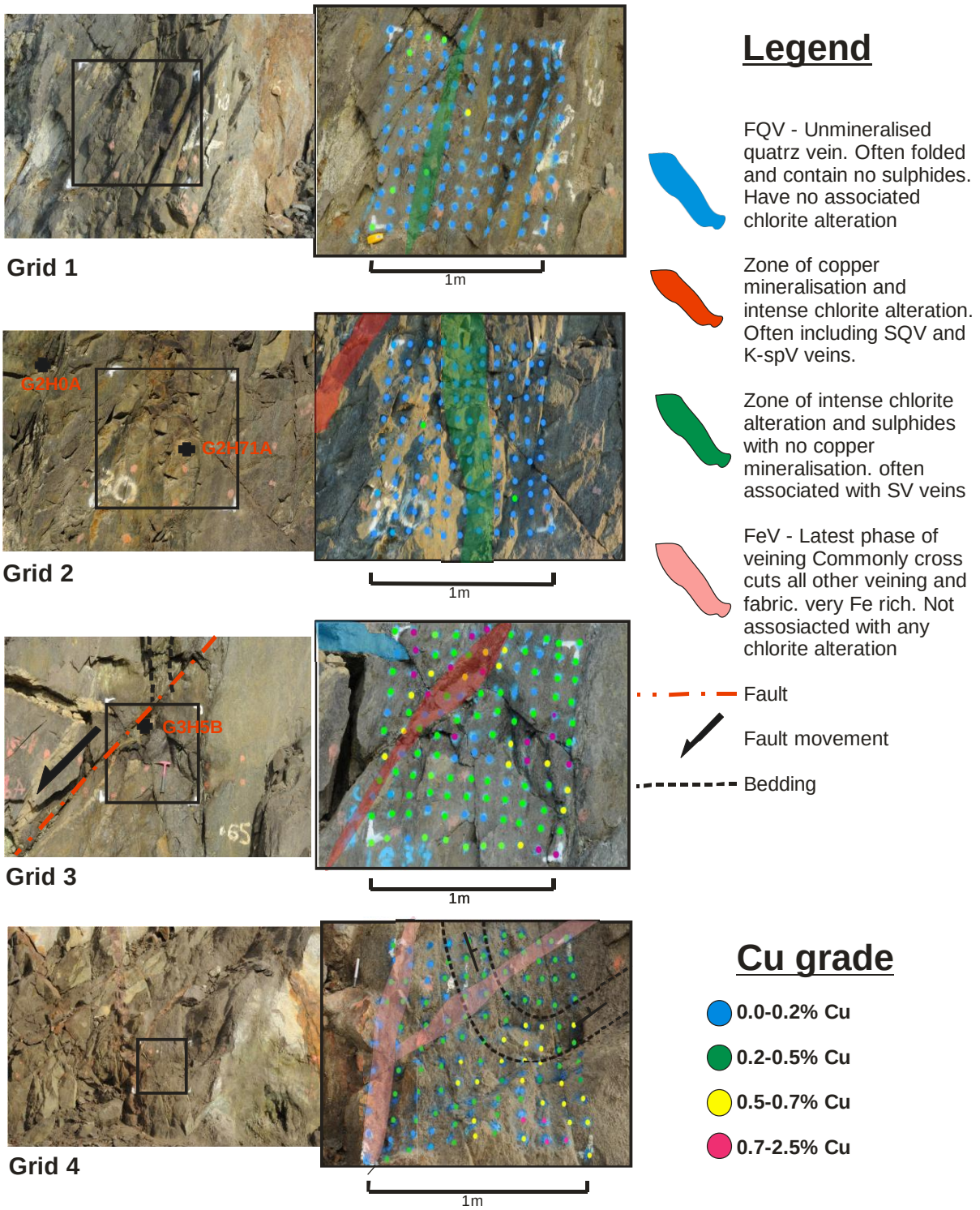

Figure 6: Close space (10cm x 10cm) handheld XRF grids 1-4 shown with blank grid vs. spot sampled overlain with Cu ppm. Figure includes locations of sampled areas (grids 2 and 3) for further petrographic, Elemental and sulphur isotope analysis. Grids were selected on the basis of intensity of chlorite alteration, veining present and the presence of key structural features. Grid 1: 15-20m – Intense chlorite alteration zone in association with SV vein indicating no mineralisation present. Grid 2: 30-35m - Intense chlorite alteration with minor SV veins, no mineralisation present. Grid 3: 60-65m – K-spV and SQV veining in association with a normal fault, intense chlorite alteration and significant Cu mineralisation. Grid 4:110-115m - Moderate chlorite alteration present across the whole grid. Moderate levels of Cu mineralisation in association with the fold hinge, but no mineralisation associated with FeV veins.

Table 4: Key features of each grid including number, location, veining, mineralisation, alteration and any other significant features. Grid 1: 15-20m – Intense chlorite alteration zone in association SV vein indicating no mineralisation present. Grid 2: 30-35m - Intense chlorite alteration with minor SV veins, no mineralisation present. Grid 3: 60-65m – K-spV and SQV veining in association with a normal fault, intense chlorite alteration and significant Cu mineralisation. Grid 4: 110-115m - Moderate chlorite alteration present across the whole grid. Moderate levels of Cu mineralisation in association with the fold hinge, but no mineralisation associated with FeV

Grid Number	Location on Mapping	Lithology	Veining Present	Cu Mineralisation	Chlorite alteration (1-5)	Other Features
1	15-20m	Biotite garnet chlorie schist	SV vein through centre of grid 5cm wide	N	4	relic andalusite present
2	30-35m	Biotite garnet chlorie schist	several SV veins 0.5-1cm wide	N	5	some zones of very coarse garnet up to 0.4cm in diameter
3	60-65m	Biotite garnet staurolite chlorie schist	large (up to 20 cm wide) K-spV, SQV	Y	5	staurolite present at contact K-spV, SQV and wallrock
4	110-115m	Garnet andalusite biotite schist ± chlorite	FeV 30 cm wide	y	2	moderate Cu present in hinge of fold however not associated with veining

CHL2, shown in grids 1 and 2 (figure 6 and table 3) has occasionally seen elevated levels of Fe, Bi and Au to be associated with this phase of alteration. Sulphides associated with CHL2 include pyrrhotite and large amounts of pyrite often seen in SV veining. In areas where copper bearing veins and CHL1 has been overprinted by CHL2, very coarse garnet growth is observed. Contacts between host rock and CHL2 are very sharp and show in immediate destruction of all other previous fabrics. These contacts are seen to be centimetres wide.

S, Fe, Al ternary plots (figure 6) from bulk XRF and close grid XRF data indicate the elevated levels of sulphur present in both mineralised and unmineralised chloritised zones. Elevated levels of sulphur and iron have been also been recorded in unmineralised, unaltered GABS (figure 6)

S, K, Al ternary plots of Bulk XRF (figure 6.) and close grids (figure7) indicate again a spread towards high sulphur values with the presence of chlorite alteration. Unmineralised chloritised schists in grids 1 and 2 show trends to more Al rich members, while mineralised grid 3 shows increased K levels. This is however most likely due to the presence of copper bearing K-feldspar veins in the grid. Grid 4 has disseminated copper mineralisation, and shows much lower levels of sulphur because of this. This grid has higher levels of K than the unmineralised, unaltered grids 1 and 2.

Co, Zr, Bi ternary plots (appendix C) indicates an association with Co and mineralised K-feldspar veins, however there is little association with copper mineralisation and Bi. Cu, Mn, Al ternary plot (figure 7) indicate a trend towards higher manganese with the presence of copper bearing and chloritised K-feldspar veins. This alteration is also present in unmineralised but chloritised grid 2.

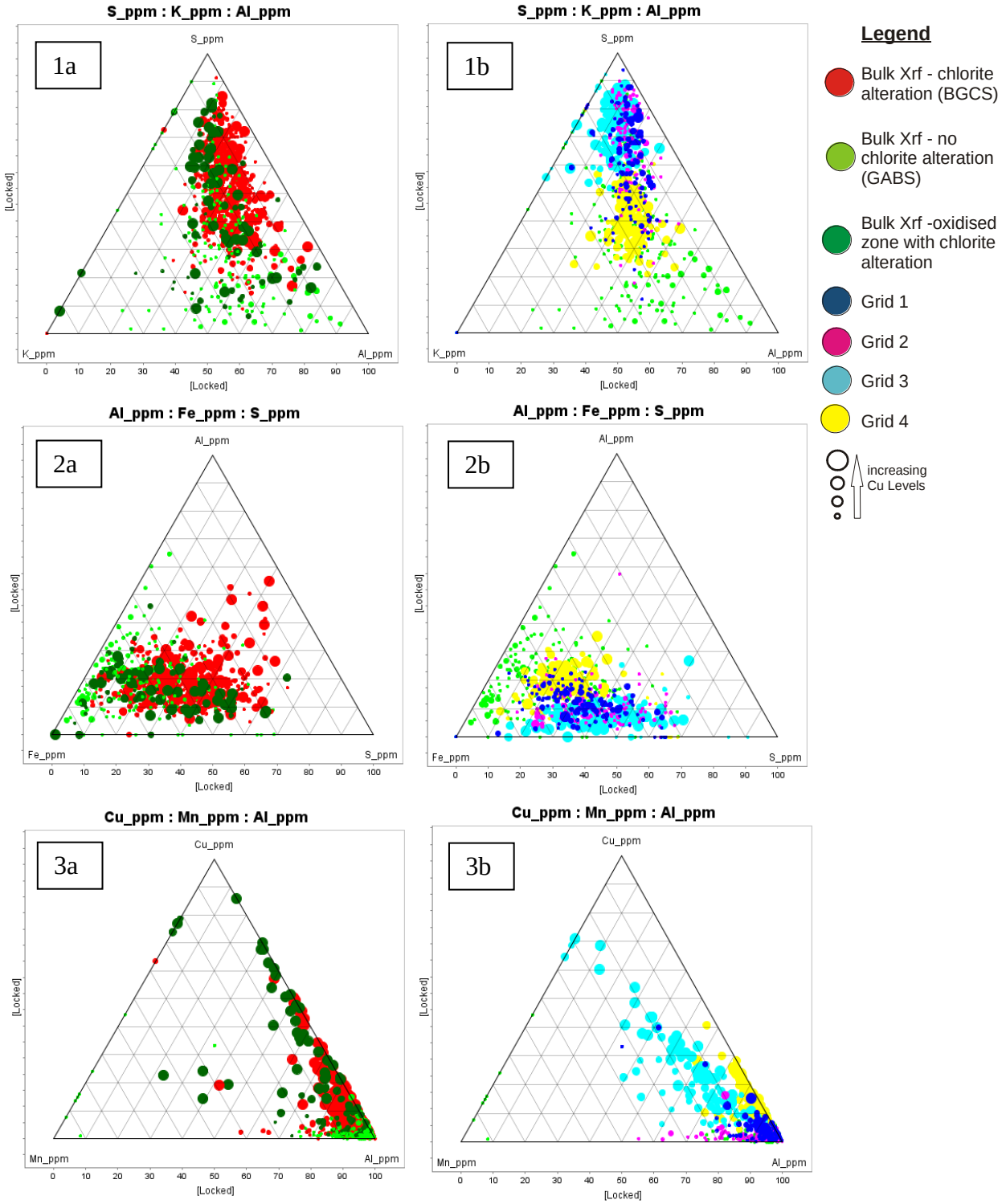

Figure 7 : Ternary plots of handheld XRF data from bulk XRF GABS v BGCS v oxidised BGCS (1a, 2a, 3a) and bulk XRF GABS vs. grids 1-4 (1b, 2b, 3b). All results are in PPM scale. 1a –S:K:Al XRF GABS v BGCS v oxidised BGCS indicating chloritised samples have a consistent trend towards high S, however some unaltered, unmineralised GABS indicate moderate to high levels of S. 1b - S:K:Al XRF GABS vs. grids indicating consistent high levels of S in both mineralised and unmineralised chloritised samples from the 4 grids. 2a –Al:Fe:S XRF GABS v BGCS v oxidised BGCS indicating consistent trends in altered sample to high S, however high Fe is consistent in GABS. 2b - Al:Fe:S XRF GABS vs. Grids indicating consistent trends in altered grid samples to high S, however high Fe is consistent in GABS. Moderate levels of Al are seen in grid 4 results due to disseminated Cu sulphides. 3a - Cu:Mn:Al XRF GABS v BGCS v oxidised BGCS indicating low levels of Mn in GABS with occasional elevated levels of Mn in mineralised samples. 3b - Cu:Mn:Al XRF GABS vs. Grids indicating positive trend towards Mn when K-spV veins are present (grid 3).

Petrology

SAMPLE SI-0-5

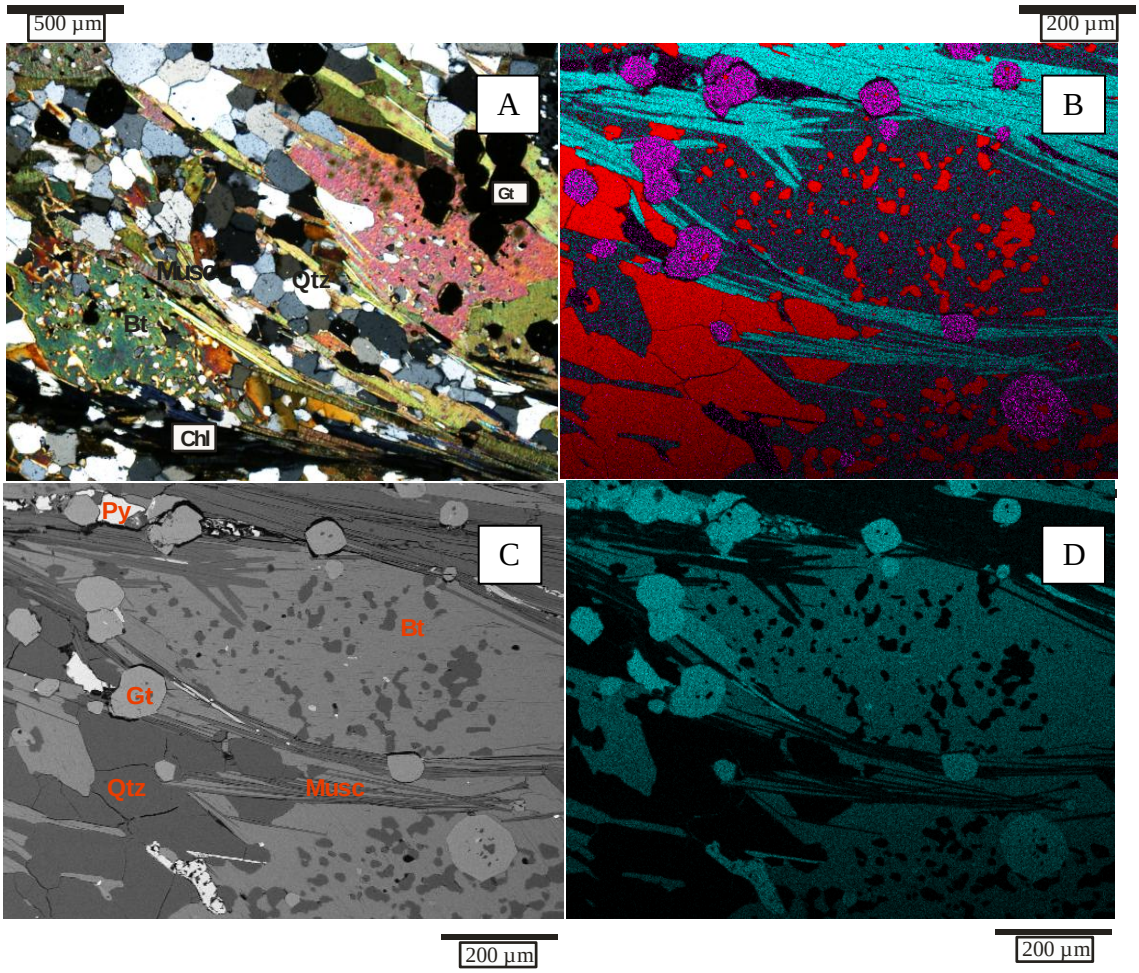

Figure 8: Sample SI-0-5 from 0 metres (figure 4) displayed as ;(A) thin section in thin cross polarised light; (B) Edax combination element map; Al (light blue), Si (red), Mn (pink); (D) Fe Edax element map. Mineral codes are - Py: pyrite, Bt: biotite, Gt: garnet, Musc: muscovite, Qtz: quartz, Chl: chlorite. The sample is characterised by biotite, abundant garnet crystals and a schistose fabric. The groundmass is quartz grains with biotite. The rock fabric is formed by elongated needle-like muscovite crystals that are tightly grouped and orientated along the S2 schistosity. Minor chlorite is seen to be overprinting biotite but less aligned with the fabric. Minor pyrite is also seen to be present within the main fabric

The sample was taken from a prominent shear zone at 0 metres in GBP lithology seen on face mapping (figure 4). The sample is characterised by biotite, abundant garnet crystals and a schistose fabric (figure 8A). The groundmass is quartz grains with biotite. The rock fabric is formed by elongated needle-like muscovite crystals that are tightly grouped and orientated along the S2 schistosity. Minor chlorite is seen to be

overprinting biotite but less aligned with the fabric. Minor pyrite is also seen to be present within the main fabric. Edax XL-40 element maps of Al, Si and Mn (figure 8B) and Fe (figure 8D) show quartz inclusions within the biotite and Mn and Fe-rich garnets aligned with the S2 foliation

SAMPLE G2H0A

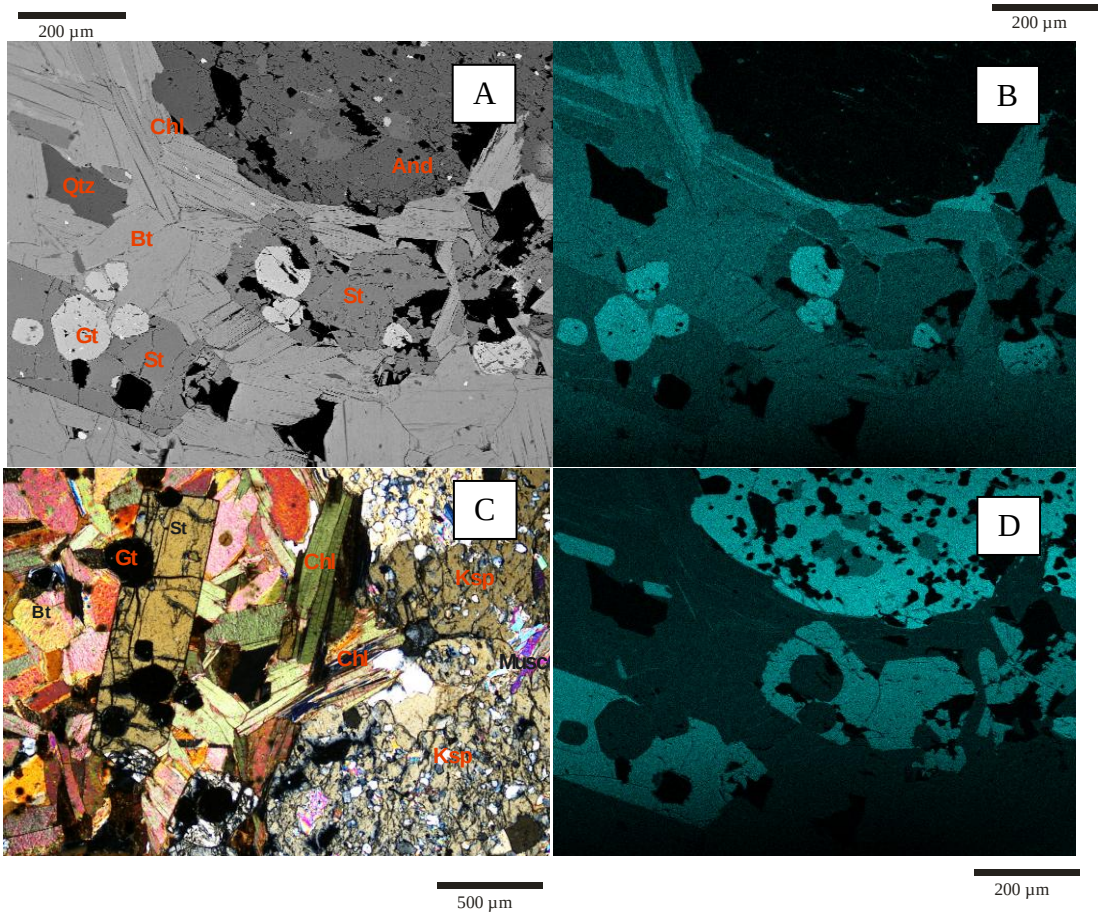

Figure 9: Sample G2H0A from metres 28-30 (figure 4, figure 6) displayed as ;(A) Edax beam image; (B) Fe Edax element map; (C) thin section in thin cross polarised light (D) Al Edax element map. Mineral codes are – And: Andalusite, Ksp: K-feldspar, St: Staurolite, Bt: biotite, Gt: garnet, Musc: muscovite, Qtz: quartz, Chl: chlorite. The sample is characterised by decussate biotite, staurolite, andalusite and garnet, with minor chlorite and quartz. Quartz inclusions are found within the andalusite grain, and staurolite is seen to post date garnet growth, as inclusions of garnet are found within the staurolite.

The sample was taken from metres 28-30 (figure 6) and was from the contact of a copper bearing K-feldspar vein and the surrounding BGCS. The sample is

characterised by decussate biotite, staurolite, andalusite and garnet, with minor chlorite and quartz. Quartz inclusions are found within the andalusite grain, and staurolite is seen to post date garnet growth, as inclusions of garnet are found within the staurolite. Edax XL-40 element maps of Al and Fe (figure 9B and 9D) quartz inclusions within the andalusite grain and Fe rich chlorite surrounding the andalusite grain. Fe rich garnets and chlorite are seen to overprint decussate biotite and the Fe poor staurolite suggesting later mineral assemblage.

SAMPLE G3H5B

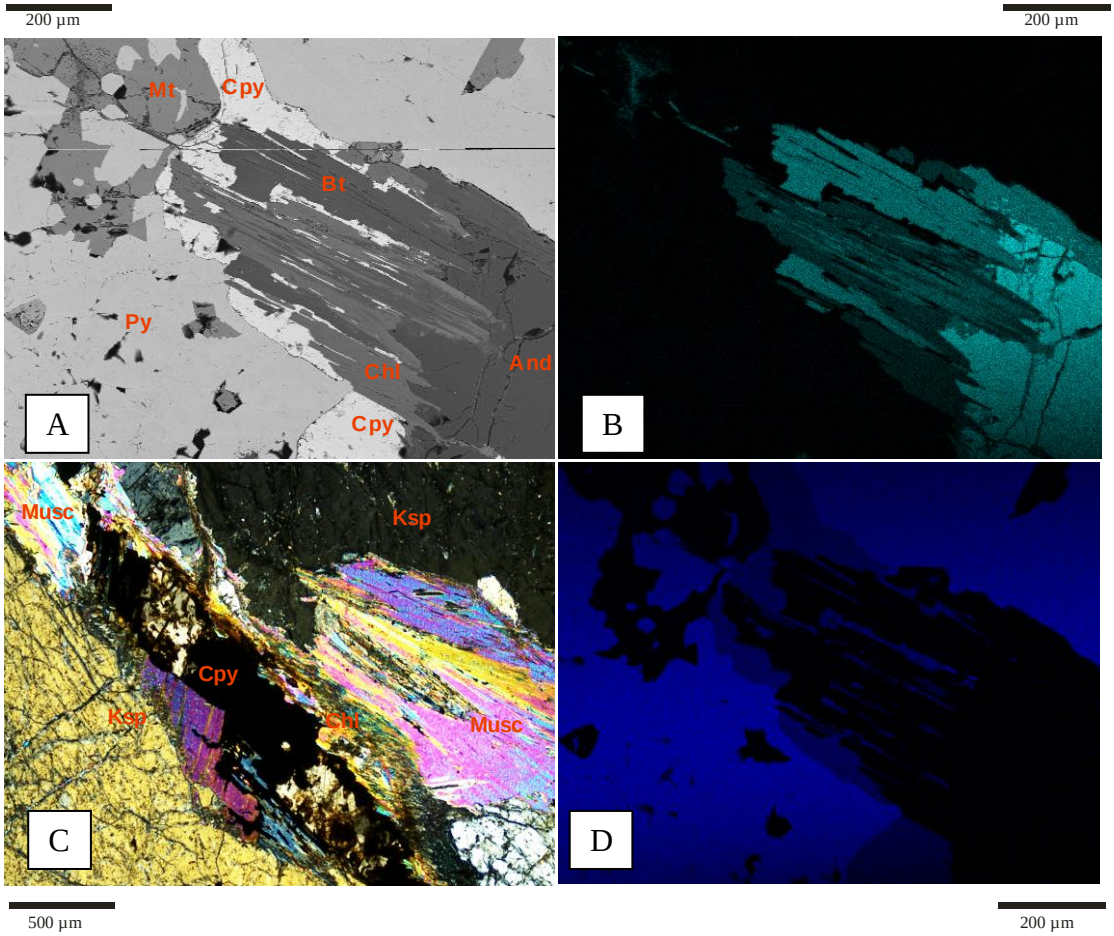

Figure 10: Sample G3H5B from metres 60-65 (figure 4, figure 6) displayed as ;(A) Edax beam image; (B) Al Edax element map; (C) thin section in thin cross polarised light ;(D) S Edax element map. Mineral codes are – And: Andalusite, Ksp: K-feldspar, St: Staurolite, Bt: biotite, Gt: garnet, Musc: muscovite, Qtz: quartz, Chl: chlorite, Py: pyrite, Cpy: chalcopyrite, Mt: magnetite. . The sample is characterised by Pyrite, magnetite and chalcopyrite in contact with biotite and andalusite. Chlorite is seen to be directly associated with chalcopyrite and replaces biotite. As chalcopyrite and chlorite infill fractures in the andalusite, it is seen to post date andalusite mineral growth. Pyrite and magnetite appear to be in equilibrium suggesting

emplacement at the same time, however chalcopyrite growth along the contact of biotite and pyrite suggest the emplacement of chalcopyrite to be a later event.

The sample was taken from metres 62-65 (figure 6) and was from a copper bearing K-feldspar vein. The sample is characterised by Pyrite, magnetite and chalcopyrite in contact with biotite and andalusite (figure 10A). Chlorite is seen to be directly associated with chalcopyrite and replaces biotite. As chalcopyrite and chlorite infill fractures in the andalusite, it is seen to post date andalusite mineral growth. Pyrite and magnetite appear to be in equilibrium suggesting emplacement at the same time, however chalcopyrite growth along the contact of biotite and pyrite suggest the emplacement of chalcopyrite to be a later event.

SAMPLE G2H71A

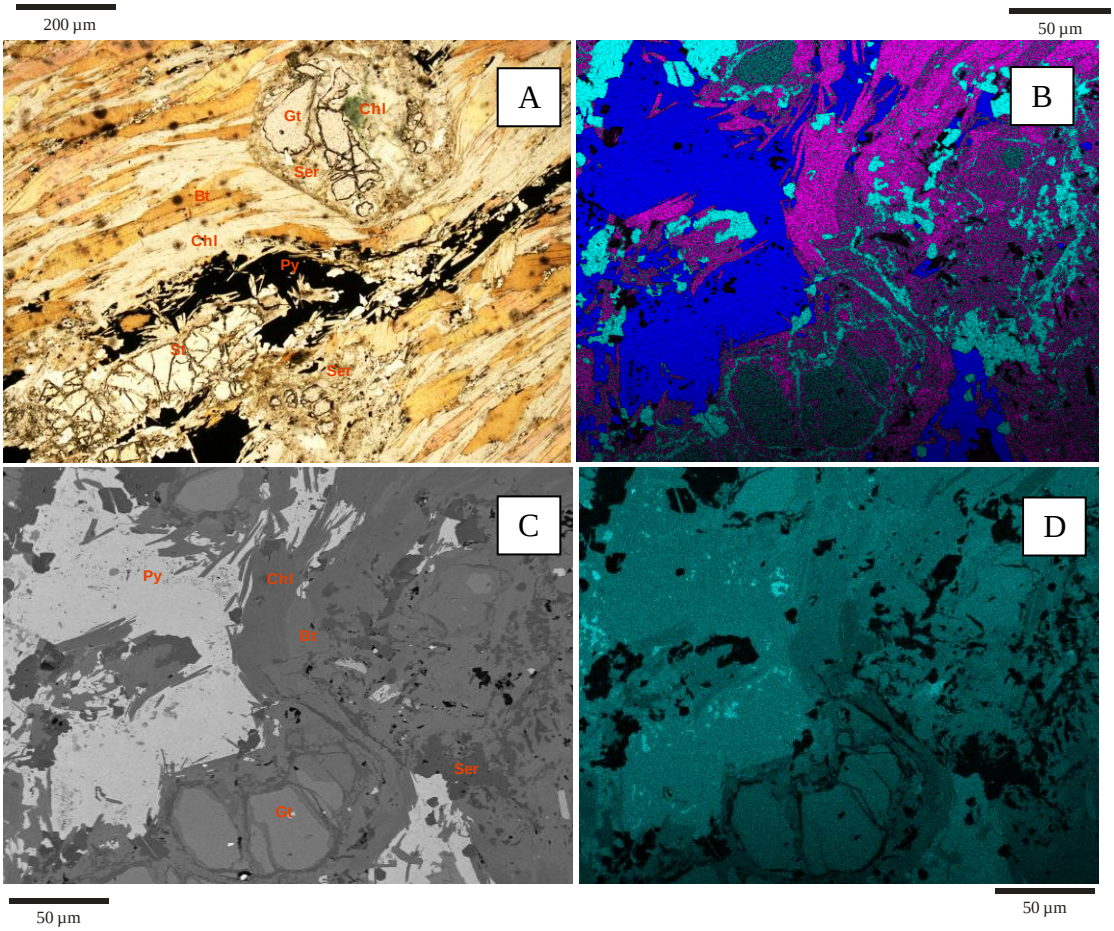

Figure 11: Sample G2H71A was taken from metres 30-35 (figure 4, figure 6) displayed as ;(A) thin section in plane polarised light; (B); Edax combined of S (dark blue), Mg (pink), Al (light blue); (C) Edax beam image;(D) Fe Edax element map. Mineral codes are – And: Andalusite, Ksp: K-feldspar, St: Staurolite, Bt: biotite, Gt: garnet, Musc: muscovite, Qtz: quartz, Chl: chlorite, Py: pyrite, Cpy: chalcopyrite, Mt: magnetite. The sample is characterised by a strong biotite fabric, with coarse grained garnets (figure...).. Chlorite is abundant and is found within garnets and is associated with biotite and sericite. Pyrite is present and is aligned along the biotite fabric. Staurolite is present and cross cuts this fabric. Edax XL-40 mapping of S, Mg and Al along with Fe shows an association between Fe rich chlorite and pyrite, as well as magnetite inclusions within the pyrite. No chalcopyrite was found within this sample.

The sample was taken from metres 30-32 (figure 4, figure 6) and was from a highly chloritised sulphide bearing vein. The sample is characterised by a strong biotite fabric, with coarse grained garnets (figure 11A). Chlorite is abundant and is found within garnets and is associated with biotite and sericite. Pyrite is present and is aligned along the biotite fabric. Staurolite is present and cross cuts this fabric. Edax XL-40 mapping of S, Mg and Al (figure 7) along with Fe (figure 7) indicates an

association between Fe rich chlorite and pyrite, as well as magnetite inclusions within the pyrite. No chalcopyrite was found within this sample.

Sulphur Isotopes

Sulphur isotope analysis was undertaken on four different veins from the 1190 RL bench. Two of these veins were copper bearing quartz veins, and two were copper bearing K-feldspar veins. The location of these veins can be seen in figure 6

SQV1 – located 0-5 metres, east of grid 1 (figure 6). Vein type SQV as outlined in table 1 above.

SQV2 - located at 59 metres, 4 metres east of grid 3 (figure 6). Vein type SQV as outlined in table 1 above.

K-spV1 - K-feldspar vein located at 29 metres, 1 metre east of grid 2 (figure 6). Vein type K-spV as outlined in table 1 above.

Ksp-V2 - K- feldspar vein located at 64 metres, and located within grid 3 (figure 6). Vein type K-spV as outlined in table 1 above.

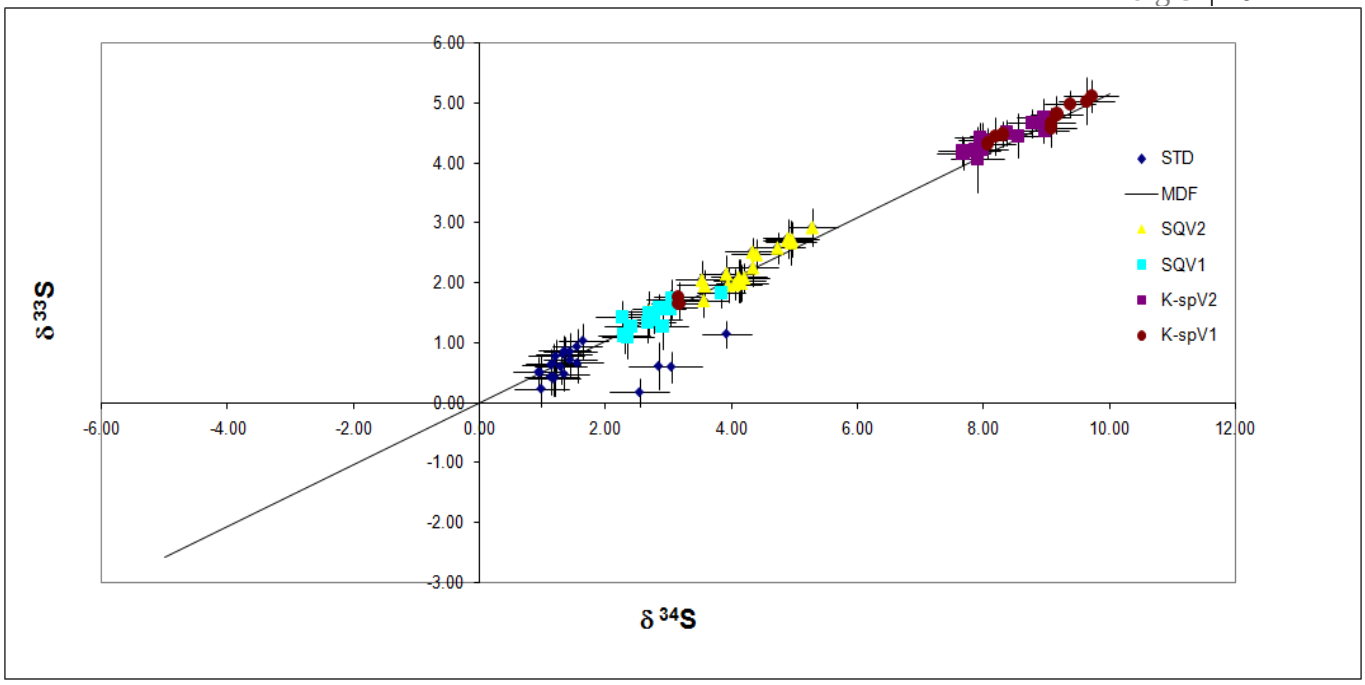

Figure 12: $\delta^{34}S$ and $\delta^{33}S$ isotope ratios for four different copper bearing veins. SQV1 shows sulphur levels of 2.1‰ up to 3.85‰. SQV2 has a spread from 3.4 ‰to 5.6 ‰. K-spV1 has a spread from 3.1‰ up to 10.2‰. K-spV2 has a range from 7.89 ‰ to 8.96 ‰. STD represents standards used and calibrated against.

SQV1 - 21 analysis points were taken from 5 separate chalcopyrite grains from quartz vein 1 . Results were consistent between 2.27 ‰ and 3.83 ‰. These were results, seen in figure 13 above were consistently the lowest permil results given for all sulphides analysed.

SQV2 - 19 analysis points were taken from 4 separate chalcopyrite grains from SQV type veins (table 1). Results were consistent between 3.83 ‰ and 5.29 ‰. These were results, seen in figure 13 above were consistently the lowest permil results given for all sulphides analysed.

K-spV1 - 20 analysis points were taken from 5 separate chalcopyrite grains from K-feldspar vein 1 (K-spV). Results were consistent between 2.67 ‰ and 9.64 ‰. These results, seen in figure 13 above had the widest range for all sulphides analysed.

K-spV2 - 18 analysis points were taken from 6 separate chalcopyrite grains from K-feldspar vein 2. Results were consistent between 7.67 ‰ and 8.96‰. These results, seen in figure 13 above were the tightest range of any of the veins analysed.

DISCUSSION

TIMING OF MINERALISATION

Tight folds that deform bedding and an earlier foliation are noted throughout the mapped face (figure 4). Oliver et al. (1998) and Abbot et al. (2005) have suggested that these folds and shear structures at the Kanmantoo mine are D3 deformation events. This folding noted, and associated garnet-andalusite-biotite mineral assemblages, has been shown to be overprinted by decussate biotite, garnet and staurolite (figure 9). Copper mineralisation, along with associated chlorite, garnet and muscovite alteration has been shown to overprint these decussate minerals which is evidence to suggest mineralisation post dates D3 folding and any shortening strain stress regimes.

Further evidence for copper mineralisation post dating D3 deformation is seen as both K-spV SQV veins as both sets have been seen to cross cut D3 fold and associated fabrics (figure 4). Tedesco (2009) analysed quartz veins similar to SQV veins and recognised that these veins do not display any signs of compressional strain and inferred that vein formation post-dated the main Delamerian phase of shortening. These observations, in conjunction with the mine scale discordance of mineralisation to bedding, strongly suggest that mineralisation was not formed as a concordant sedimentary hosted deposit during the rifting stage of basin evolution as suggested by Seccombe (1985).

Oliver et al. (1998) and Schiller (2000) suggested that mineralisation occurred at peak metamorphic conditions. This was based on the observation that some mineralisation could be associated with peak metamorphic assemblages. Tedesco (2009) and Arbon (2011) showed mineralised quartz veining similar to SQV veins in this study, were formed at lower

temperatures. Tedesco (2009) produced TitaniQ results of quartz veins showing a temperature range of 355 to 395°C, and Arbon (2011) also suggested that the chlorite associated with these veins formed under temperatures of around 400^{o}C. These temperature estimates given by Tedesco (2009) and Arbon (2011) are 150 to 200°C lower than previous estimates based on biotite-garnet-staurolite bearing peak metamorphic mineral assemblages associated with D3 deformation. Previous workers (Seccombe, 1986, Schiller 2000..) recognised an association with mineralisation and both parasitic and major fold limbs and hinges throughout the Kanmantoo pit. These findings lead to a suggestion that mineralisation was either pre or syn compression. In this study mineralised SQV veins are found as metre scale pods localized in the hinges of D3 antiforms. An example of this can be seen in figure 4 between metres 59 to 64, directly adjacent to a normal fault.

Wilson (2009) suggests reactivation of east dipping compressional fault planes with normal movement, seen only at camp scale, are pathways and controls for localising mineralising fluids. The normal fault seen between metres 60-64 (figure 4 and figure 6) supports this finding as mineralised K-spV and SQV veins are seen to be closely associated with this zone. In-situ U-Th-Pb dating by Wilson (2009) determined mineralised veins, similar to SQV veins in this study, at 492±9 Ma. The shallow angle of the fault zone, along with tight D3 folding seen on the hanging wall of this fault zone is consistent with the geometry of a D3 reverse fault reactivated as a normal fault during the extensional phase.

The location within these antiformal zones could suggest that these D3 axial planes acted as a conduit and trap for later mineralizing fluids which entered the Kanmantoo system via the extensional reactivation of D3 compressional shear structures mentioned previously. This style of veining and relationship to D3 antiforms has been recognised by Hillgrove Resources

mine geologists elsewhere in the mine, however due to access issues, these zones could not be included in this paper.

Studies by Foden et al. (2006), have shown the emplacement of a series A-type granites and mafic intrusions occurred at the termination of the Delamerian Orogeny, dated at 490 ±3 Ma (). This magmatism occurred during the first phases of post-orogenic extension which is interpreted to be driven by slab-rollback and extensional orogenic collapse (Foden et al. 2006).

Focke (2010) gives ages of 469 ± 17 Ma from U-Th-Pb dating for mineralisation of the gold dominant O'Neil satellite deposit. Latest resource modelling by Hillgrove resources (2012) shows that the O'Neil deposit strikes NE-SW. This orientation is consistent with the second generation, later phase SV veins and associated chlorite alteration (average dip/dip direction of 84/115 on the 1190 RL bench). Very minor Au and Bi was detected by handheld XRF analysis, however these rare detections were commonly associated with these SV veins. This finding supports the younger ages of gold mineralisation given by Focke (2010), and the later phase, lower temperature; gold-bismuth associated chlorite alteration given by Arbon (2011).

Franklyn (2009) studied East-West striking veins similar to that of FeV veins in this study, and concluded that these veins were not associated with any mineralisation. This study, like Franklyn (2009) suggests this phase of veining is the latest veining event recorded at Kanmantoo cross cutting all other fabrics and veins. This rotation of veins (figure 5F) suggest a rotating strain regime during orogenic collapse from initial E-W extension at 490 ±3 Ma, with mineralised SQV an K-spV veins, to unmineralised SV veins to almost N-S extension concluding with unmineralised FeV veins.

ASSOCIATED ALTERATIONS

Mapping on the 1190RL bench shows 140m wide zone of chlorite alteration of variable intensity (figure 4). Cu mineralisation occurs within discrete zones associated with SQV and K-spV veins and intense chlorite and staurolite alteration. Later phase SV veins and associated chlorite alteration (average dip/dip direction of 84/115) have indicated a minor association with Au and Bi. This is consistent with the two phases of chlorite mapped supports Arbon (2011), who first suggested two separate phases of mineralisation and alteration are involved in the Kanmantoo deposit. The study suggested that copper + base metal mineralisation pre-dated gold mineralisation. Arbon (2011) also suggested that the earliest phase of chlorite was Fe and Mg rich and formed under temperatures of around 400^{o}C, where as the later phase; gold-bismuth related chlorite was formed under lower temperatures of around 300^{o}C. These are much lower than the 550 ^{o}C temperatures estimated by Oliver et al. (1998).

Oliver et al (1998) suggests that copper mineralisation and associated chlorite alteration is coupled with Fe-rich metasomatism associated with an injection of high temperature Fe-rich fluids and formation of metasomatic decussate biotite and staurolite. Decussate chlorite-garnet-muscovite alteration associated with copper mineralisation has been shown in this study to overprint the decussate biotite and staurolite, placing mineralisation after this metasomatic event. Geochemical results of this study also show no systematic relationship between Fe and Cu concentrations. Background Fe concentrations of 5-10% occur throughout mapped 1190 RL, including unmineralised, foliated GABS schist outside the alteration zones. This study also finds significant levels of early Fe Sulphides present in unaltered, unmineralised GABS shown in face mapping (figure 4) and as seen in thin section SI-0-5 (figure 8). This finding presents an alternative to the Oliver et al. (1998) Fe metasomatic

event where mineralisation and associated chlorite alteration was a result of high temperature copper bearing fluids being injected into the Kanmantoo System and interacting with already Fe rich sediments.

SOURCE OF MINERALISING FLUIDS

Workers over several decades have debated the source of mineralising fluids at the Kanmantoo deposit. Oliver et al (1998) suggests that copper mineralisation is associated with Fe rich metasomatism associated with an injection of high temperature, igneous derived fluid during D3 deformation. Tedesco (2009) suggested an igneous source for mineralisation as his study of veins similar to SQV revealed very saline, igneous derived inclusions. Seccombe (1985) suggested a mixing with biogenic sulphur and Cambrian sea water after a study into the sulphur isotopes at the site.

The discovery of copper bearing K-feldspar veins in this study strongly supports an igneous source for mineralising fluids. Tedesco (2009) showed static modelling of saline fluids at temperatures of ~ 420°C results in an increase of magnetite production. Figure 10 shows magnetite and chalcopyrite, along with cobalt and molybdenum is present within these K-spV K-feldspar veins. The presence of magnetite in these K-feldspar veins is suggestive of a slightly oxidised, magnetite bearing magmatic fluid, possibly from magnetite series granite. Elevated levels of Mo and Co in association with copper mineralisation were recognised by Arbon (2011) to link mineralisation to an igneous intrusive. The elevated levels of Mo and Co that are present in these mineralised K-feldspar veins seen in this study are further supports an igneous source for mineralising fluids.

Arguments could be made that these copper bearing K-feldspar veins could be as a result of local re-mobilisation of K and AL, allowing the precipitation of K-feldspar into voids in the rock. This theory is dismissed however due to the low levels of K and AL mobilisation in deformation and metamorphism seen in XRF results across the mapped face and close spaced grids and it is determined that these veins are derived from an external, igneous source.

$\delta^{34}S$ Sulphur isotope results of 2.21‰ to 9.23‰ obtained in this study (figure 13) were similar to results given by Seccombe (1985). Seccombe (1985) suggested that the Sulphur isotopes were derived from deep (3-4 km minimum) convective circulation or seismic pumping of Cambrian seawater at (+30 ‰) (Ohmoto and Rye 1979), mixing with the Sulphur from the Tapanappa formation (19‰ to -16‰) subsequently discharging onto the basin floor at the time of accumulation of Kanmantoo Group sediments. Seccombe (1985) dismissed an igneous source on the basis that there were no recognised magmatic rocks of the appropriate age at the time of his study. Oliver (1998) pointed out that due to the low levels of sulphur in sea water compared to the Tapanappa sediments unrealistic fluid - rock ratios would be required to obtain the sulphur levels seen at Kanmantoo. As an alternative Oliver et al. (1998) suggested an igneous source for the mineralising fluid which is supported by an oxygen isotope study completed by Oliver et al. (1998). Ranges for fluids obtained by Oliver et al. (1998) were between 6.4‰ to 9.3‰ permil which are most suggestive of a fluid being released from a crystallising magma.

Early studies by Vinogradov (1958) and Thode et al. (1961) recognized that the sulphur isotopic composition of the mantle and mantle derived igneous rocks is close to 0 ± 2‰ (figure 13). This would suggest another influence or a fluid mixing reaction to have taken place to obtain sulphur values between 2.21‰ and 9.23‰ permil if the sulphur at Kanmantoo

has an igneous source. Recent work on sulphur isotope signatures of post-collisional granitoids in central Anatolia, Turkey (Boztug and Arehart 2006) shows that I-type and A-type granitoids contain a significant crustal contribution reflected in $\delta^{34}S$ between 3‰ and 9‰ (figure 14). The study suggested source materials may include a metasomatised mantle layer that was affected by supra-subduction zone-derived fluids before the Neo-Tethyan collision in central Anatolia (Boztug and Arehart 2006). The study has suggested that an accretion of a metasomatised mantle layer into the sub continental lithosphere during collision, which was followed by partial melting in the post-collisional extensional tectonic setting that was maintained by slab break-off or lithospheric delamination mechanisms.

Foden (2002) has suggested a similar supra-subduction related mantle metasomatism during subduction during the Delamerian Orogeny. This in turn has allowed for crustally contaminated mantle to be emplaced place during the latest stages of the Delamerian Orogeny and during post orogenic extension (figure 14). This is, along with the presence of Cu, Mo, Co, and magnetite in K-feldspar K-spV veins, oxygen isotopes completed by Oliver et al. (1998) and sulphur isotope results gained from to strongly suggest an igneous source for mineralising fluids at Kanmantoo.

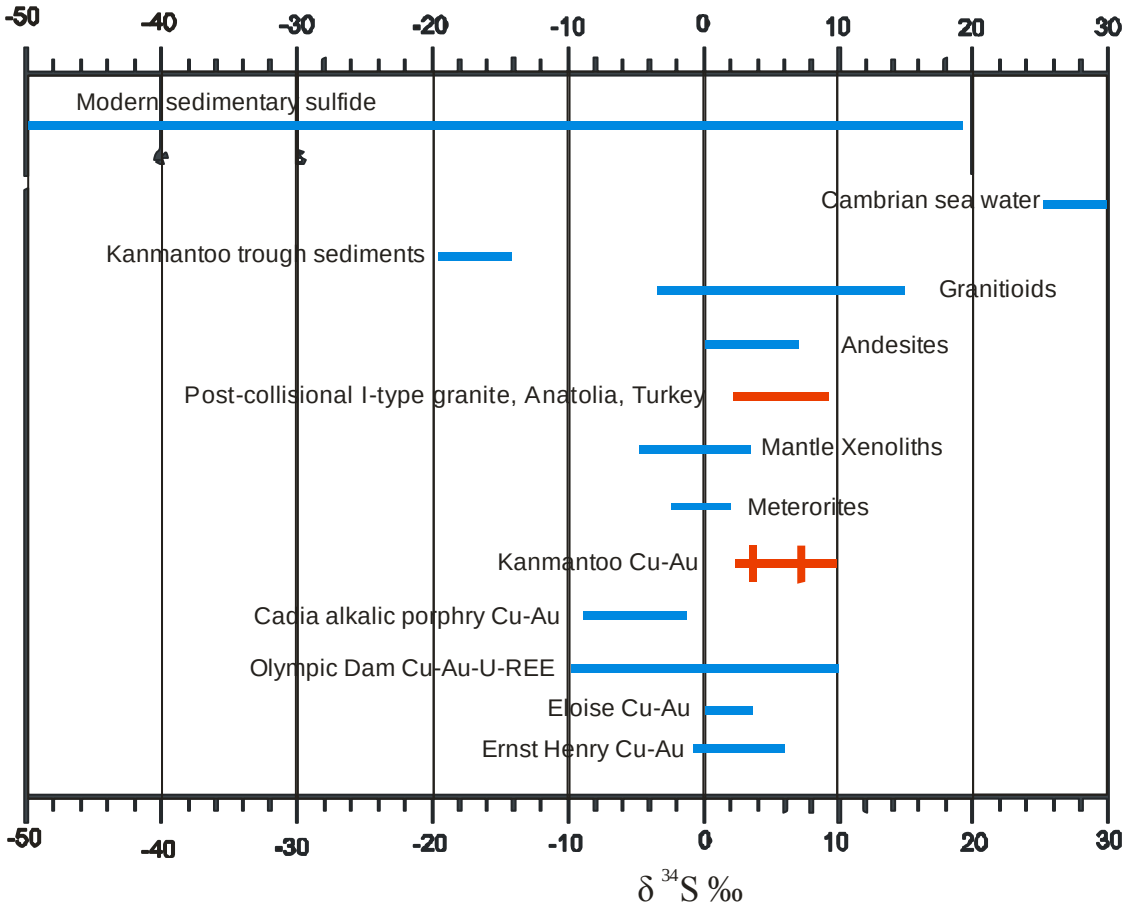

Figure 13: Adapted from Marini et al (2011) showing Range of sulphur isotope values for sulphides from meteorites, mantle xenoliths, igneous rocks and modern sediments. δ ^{34}S isotope values from Kanmantoo Cu-Au deposit and post-collisional I-type granites from Anatolia, Turkey are highlighted in red. (Data from Sasaki and Ishihara 1979; Chambers 1982; Rye et al. 1984; Sakai et al. 1984; Chaussidon et al. 1987, 1989; Ishihara and Sasaki 1989; Torssander 1989; Eldridge et al. 1991; Santosh and Masuda 1991; Salen et al 1993; Strauss 1997; Farquhar et al. 2002; Luhr and Logan 2002).The δ34S value of dissolved sulphate in present-day oceans is also shown (Rees et al. 1978).

The exact location of an igneous source has been rarely mentioned by workers however Oliver et al. (1998) has suggested a source may be an igneous intrusion located at depth directly under the deposit. Gum (1998) has also suggested a source may be the Monarto granite, which is the nearest outcropping granite 10km east from the Kanmantoo mine. Interestingly this granite has been associated with the Monarto copper prospects, which are small 1860's copper workings that have the identical garnet-staurolite-andalusite assemblages as Kanmantoo (Barnes, 1971). Most notably the Monarto copper prospect has a series of felsic dykes and quartz veining associated with copper mineralisation (Barnes, 1971). Only

minor pyrite is seen in the sedimentary packages which host the mineralisation and this is attributed by Barnes (1971) to be the reason for only small levels of copper mineralisation.

Stepwise zircon evaporation 207Pb/206Pb age analysis of the Monarto granites by Foden (2006) states a primary crystallisation age of 506 ± 1 Ma, however a recrystallisation at 492 ± 6 Ma is given for the Monarto granite which is the same time given for the Reedy Creek granodiorite 492 ± 6 Ma, and the Reedy Creek diorite 491 ± 1 Ma (Foden et al. 2006) located 15 km north-east of the Kanmantoo deposit. This late Delamerian increased I-type magmatism immediately preceding the first phases of post –orogenic extension coincides very closely to mineralisation dates of 492±9 Ma given by Wilson (2009).

The results of this sulphur isotope study show two distinctive spreads of data with the first population of sulphur in SQV veins, between 2.21‰ and 5.29‰. The second population of sulphur from chalcopyrite grains in K-feldspar veins (K-spV) reside between 7.91‰ and 9.23‰. These two clusters, from differing vein lithologies could be the result of the precipitation of sulphur, and associated copper, as the fluid cools (Ohmoto and Lasaga, 1982). Further evidence for this is the initial precipitation of K-feldspar K-spV veins ($\delta^{34}S$ 7.5 ‰-9.4‰), which have been cross cut by slightly younger mineralised SQV veins ($\delta^{34}S$ 2.2 ‰ - 5‰), showing this reduction in temperature and $\delta^{34}S$ values. These results are consistent with the theory that the injection of high temperature copper bearing magmatic derived fluids cooled due to interaction and circulation with the surrounding rock, allowing differing styles of mineralisation desirable temperature and REDOX reactions are reached, seen in differing vein lithologies (K-spV, SQV) and alterations (SV, CHL1, CHL2). This may also allow for broad regions (100-200m scale) of unmineralised chlorite alteration.

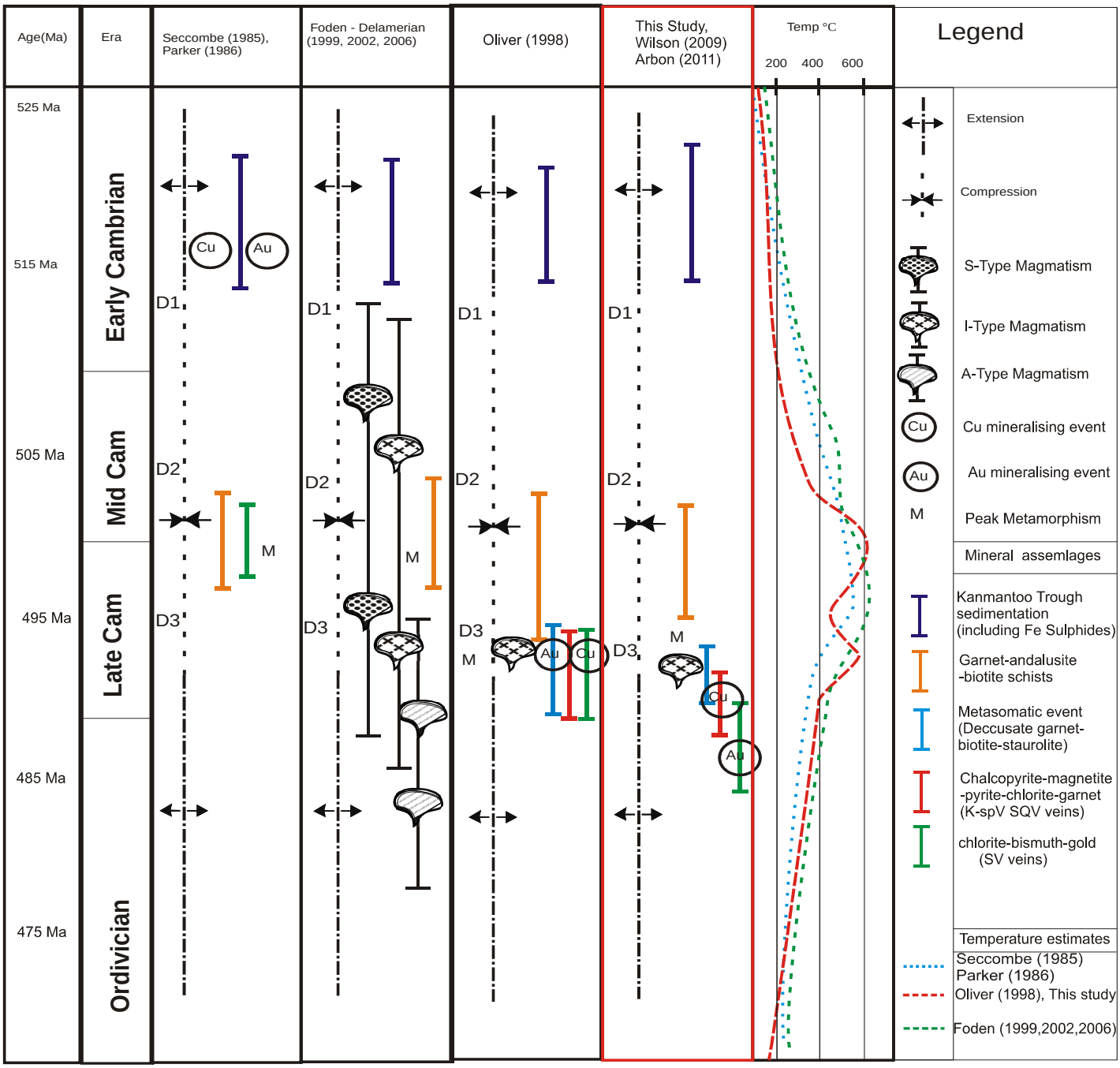

Figure 14: Various workers interpretations on the deformation events of the Delamerian Orogeny and Kanmantoo Trough including timing of mineralisation at the Kanmantoo Cu-Au Deposit, against this study (highlighted in red). Timing of Cu and Au mineralisation, along with mineral assemblages and alterations stated by workers have been highlighted and placed within a tectonic regime, timing of the Delamerian Orogeny and in relation to magmatism associated with the Delamerian Orogeny and estimated temperature. Data on timing of magmatic events have been gathered from Foden et al. (1999, 2002, 2006). Authors contributing to the establishment of shortening D1, D2 and D3 events, peak metamorphism and temperatures are : Offler and Fleming (1968), Mancktelow (1981, 1990), Parker (1986), Spry et al. (1988), Both (1990) and Preiss (1995). Structural investigations by Jenkins and Sandiford (1992), Flöttmann and James (1992), Flöttmann et al. (1994) and Marshak and Flöttmann (1996). Data gathered on mineralisation at the Kanmantoo Cu-Au deposit are from Seccombe (1985), Parker (1986), Oliver et al. (1998), Schiller (2000), Tedesco (2009), Wilson (2009) and Arbon (2011)

CONCLUSION; MODEL FOR MINERALISATION

From cross-cutting relationships and the geochemical and mineralogical results obtained from this study, along with previous studies on the Kanmantoo copper deposit and the Delamerian Orogeny (stated below conclusion), a model for mineralisation can be constructed with respect to relative timing of key structural, metamorphic and magmatic events prior to, during and post Delamerian Orogeny (Figure 14).

- 525-515 Ma Initial high levels Fe are present in the early GABS rock type metasediments of the Kanmantoo trough.

- 514 Ma - 492 ± 6 Ma. Onset of the Orogeny is initiated by westward subduction. D1, D2 and D3 folding and shortening/shearing events occur regionally, however only D3 events are seen at the Kanmantoo mine, namely the Kanmantoo mine synform, with related parasitic folds, and D3 shortening shear zones. Early biotite is seen in D2 fabrics along with quartz, andalusite with minor staurolite at peak metamorphism during D3 at ~ 550^{o} C. Syn-orogenic S and I type granites are emplaced throughout the duration of the Orogeny. Supra-subduction related mantle metasomatism occurs during subduction throughout the Delamerian Orogeny.

- 492 ± 6 Ma. Termination of the Delamerian Orogeny from rapid exhumation due to slab-rollback. Initial east-west extension and extensional re-activation of D3 shear structures is seen at the Kanmantoo deposit. Magmatic fluid from the crystallisation of post-collisional I-type granites (Magnetite-pyrite-chalcopyrite assemblage), similar to those seen at Reedy Creek, enters the Kanmantoo system. Sulphur Isotopes indicate

an igneous I-type crystallising magma as the most likely source of the sulphur. Infiltration of high temperature fluids at low differential stress results in the growth of decussate staurolite and biotite. The interaction of the fluid with the wall rock at decreasing temperatures results in a broad zone of chlorite alteration with little copper mineralisation.

A reduction in the temperature of circulating magmatic fluids to approximately 380 degrees allows for the precipitation of Cu in K-spV and SQV veins within and adjacent to reactivated D3 shears and D3 antiformal zones. Muscovite, garnet and chlorite alteration is associated with Cu mineralisation, and occurs during the formation of magnetite-pyrite assemblages and continuing slightly after. Cu precipitation is as a result of a REDOX reaction with already Fe rich sediments, and partially oxidised fluids interacting with a reducing environment, rather than being directly associated with Fe rich metasomatism.

- 469 ± 17 Ma. A rotation of the extensional stress field and reduction in temperature with continuing chlorite alteration and circulation of Magmatic fluids allowing for the possible gold precipitation in north east-south west striking structures. This relationship is recognised as sulphide veining (SV) is seen to cross cut earlier Cu bearing north-south structures and veins. This orientation for gold mineralisation is supported by the north east-south west orientation of the gold dominant O'Neil Lode which has a later date of mineralisation. Bismuth has been recognised to be associated with this event as bismuth and associated chlorites has shown lower cooling temperatures to Copper and associated chlorites.

- Full 90 degree rotation of the extensional stress occurs allowing for north-south extension. Unmineralised east – west striking veins (FeV) are seen to cross cut all structures and dated to be the last veining event in the area.

Data on timing of magmatic events have been gathered from Foden et al. (1999, 2002, 2006). Authors contributing to the establishment of shortening D1, D2 and D3 events, peak metamorphism and temperatures are : Offler and Fleming (1968), Mancktelow (1981, 1990), Parker (1986), Spry et al. (1988), Both (1990) and Preiss (1995). Structural investigations by Jenkins and Sandiford (1992), Flöttmann and James (1992), Flöttmann et al. (1994) and Marshak and Flöttmann (1996). Data gathered on mineralisation at the Kanmantoo Cu-Au deposit are from Seccombe (1985), Parker (1986), Oliver et al. (1998), Schiller (2000), Tedesco (2009), Wilson (2009) and Arbon (2011).

ACKNOWLEDGMENTS

This honours project would not have been possible without the assistance and support of the board and staff at Hillgrove Resources. Their collaboration with the Playford Trust in graciously providing me with a personal scholarship along with a separate project scholarship majorly contributed to the facilitating of this project. The on-site assistance from the mine geologists, in particular Hayden Arbon, Rupert Verco, Marie Jamiea, Michaela Wright and Alan Day. Adelaide University Staff from the Earth & Environmental Sciences faculty, in particular my supervisors Dave Giles and Alan Collins, who provided constant direction and support which I am most grateful for. Many thanks to peer reviewers Owen Girardi, Angus Tod and Joel Kirk. Thanks must also go to Ben Wade and Angus Netting from Adelaide Microscopy along with John Cliff from University of Western Australia from AMDEL for often going out of their way to provide assistance with micro-analytical techniques.

REFERENCES

ARBON H. 2011. BISMUTH DISTRIBUTION IN THE CU-AU MINERALISATION OF THE KANMANTOO DEPOSIT, SOUTH AUSTRALIA

ALBARÈDE F. 2004. THE STABLE ISOTOPE GEOCHEMISTRY OF COPPER AND ZINC. *REVIEWS IN MINERALOGY AND GEOCHEMISTRY* 55, 409-427.

ARRIBAS JR A. 1995. CHARACTERISTICS OF HIGH-SULFIDATION EPITHERMAL DEPOSITS, AND THEIR RELATION TO MAGMATIC FLUID. *MAGMAS, FLUIDS, AND ORE DEPOSITS* 23.

BAKER T., PERKINS C., BLAKE K. & WILLIAMS P. 2001. RADIOGENIC AND STABLE ISOTOPE CONSTRAINTS ON THE GENESIS OF THE ELOISE CU-AU DEPOSIT, CLONCURRY DISTRICT, NORTHWEST QUEENSLAND. *ECONOMIC GEOLOGY* 96, 723-742.

BIERLEIN F., ASHLEY P. & SECCOMBE P. 1996. ORIGIN OF HYDROTHERMAL CU・ZN・PB MINERALISATION IN THE OLARY BLOCK, SOUTH AUSTRALIA: EVIDENCE FROM FLUID INCLUSIONS AND SULPHUR ISOTOPES. *PRECAMBRIAN RESEARCH* 79, 281-305.

BOZTUĞ D. & AREHART G. B. 2007. OXYGEN AND SULFUR ISOTOPE GEOCHEMISTRY REVEALING A SIGNIFICANT CRUSTAL SIGNATURE IN THE GENESIS OF THE POST-COLLISIONAL GRANITOIDS IN CENTRAL ANATOLIA, TURKEY. *JOURNAL OF ASIAN EARTH SCIENCES* 30, 403-416.

BRUGGER J., OGIERMAN J., PRING A., WALDRON H. & KOLITSCH U. 2006. ORIGIN OF THE SECONDARY REE-MINERALS AT THE PARATOO COPPER DEPOSIT NEAR YUNTA, SOUTH AUSTRALIA. *MINERALOGICAL MAGAZINE* 70, 609-627.

CAMECA 2012. CAMECA IMS 1280-HR, ULTRA HIGH SENSITIVITY MAGNETIC SECTOR SIMS FOR GEOSCIENCES <http://www.cameca.com/instruments-for-research/ims1280.aspx>**. (RETRIEVED 15/09/2012).**

COOK N. J. & HOEFS J. 1997. SULPHUR ISOTOPE CHARACTERISTICS OF METAMORPHOSED CU・(ZN) VOLCANOGENIC MASSIVE SULPHIDE DEPOSITS IN THE NORWEGIAN CALEDONIDES. *CHEMICAL GEOLOGY* 135, 307-324.

DAILY B. & MILNES A. 1972. REVISION OF THE STRATIGRAPHIC NOMENCLATURE OF THE CAMBRIAN KANMANTOO GROUP, SOUTH AUSTRALIA. ***JOURNAL OF THE GEOLOGICAL SOCIETY OF AUSTRALIA*** **19, 197-202.**

DING T., VALKIERS S., KIPPHARDT H., DE BIÈVRE P., TAYLOR P. D. P., GONFIANTINI R. & KROUSE R. 2001. CALIBRATED SULFUR ISOTOPE ABUNDANCE RATIOS OF THREE IAEA SULFUR ISOTOPE REFERENCE MATERIALS AND V-CDT WITH A REASSESSMENT OF THE ATOMIC WEIGHT OF SULFUR. ***GEOCHIMICA ET COSMOCHIMICA ACTA*** **65, 2433-2437.**

FINN C., MOORE D., DAMASKE D. & MACKEY T. 1999. AEROMAGNETIC LEGACY OF EARLY PALEOZOIC SUBDUCTION ALONG THE PACIFIC MARGIN OF GONDWANA. ***GEOLOGY*** **27, 1087-1090.**

FLOETTMANN T., HAINES P., JAGO J., JAMES P., BELPERIO A. & GUM J. 1998. FORMATION AND REACTIVATION OF THE CAMBRIAN KANMANTOO TROUGH, SE AUSTRALIA; IMPLICATIONS FOR EARLY PALAEOZOIC TECTONICS AT EASTERN GONDWANA'S PLATE MARGIN. ***[SERIAL] JOURNAL OF THE GEOLOGICAL SOCIETY OF LONDON*** **155, 525-539.**

FLÖOTTMANN T., GIBSON G. M. & KLEINSCHMIDT G. 1993. STRUCTURAL CONTINUITY OF THE ROSS AND DELAMERIAN OROGENS OF ANTARCTICA AND AUSTRALIA ALONG THE MARGIN OF THE PALEO-PACIFIC. ***GEOLOGY*** **21, 319-322.**

FLÖTTMANN T., HAINES P., JAGO J., JAMES P., BELPERIO A. & GUM J. 1998. FORMATION AND REACTIVATION OF THE CAMBRIAN KANMANTOO TROUGH, SE AUSTRALIA: IMPLICATIONS FOR EARLY PALAEOZOIC TECTONICS AT EASTERN GONDWANA'S PLATE MARGIN. ***JOURNAL OF THE GEOLOGICAL SOCIETY*** **155, 525-539.**

FLÖTTMANN T., JAMES P., ROGERS J. & JOHNSON T. 1994. EARLY PALAEOZOIC FORELAND THRUSTING AND BASIN REACTIVATION AT THE PALAEO-PACIFIC MARGIN OF THE SOUTHEASTERN AUSTRALIAN PRECAMBRIAN CRATON: A REAPPRAISAL OF THE STRUCTURAL EVOLUTION OF THE SOUTHERN ADELAIDE FOLD-THRUST BELT. ***TECTONOPHYSICS*** **234, 95-116.**

FODEN J., BAROVICH K., JANE M. & O'HALLORAN G. 2001. SR-ISOTOPIC EVIDENCE FOR LATE NEOPROTEROZOIC RIFTING IN THE ADELAIDE GEOSYNCLINE AT 586 MA: IMPLICATIONS FOR A CU ORE FORMING FLUID FLUX. ***PRECAMBRIAN RESEARCH*** **106, 291-308.**

FODEN J., ELBURG M. A., DOUGHERTY-PAGE J. & BURTT A. 2006. THE TIMING AND DURATION OF THE DELAMERIAN OROGENY: CORRELATION WITH THE ROSS OROGEN AND IMPLICATIONS FOR GONDWANA ASSEMBLY. ***THE JOURNAL OF GEOLOGY*** **114, 189-210.**

FODEN J., SANDIFORD M., DOUGHERTY-PAGE J. & WILLIAMS I. 2009. GEOCHEMISTRY AND GEOCHRONOLOGY OF THE RATHJEN GNEISS: IMPLICATIONS FOR THE EARLY TECTONIC EVOLUTION OF THE DELAMERIAN OROGEN. ***AUSTRALIAN JOURNAL OF EARTH SCIENCES*** **46, 377-389.**

FODEN J., SONG S. H., TURNER S., ELBURG M., SMITH P., VAN DER STELDT B. & VAN PENGLIS D. 2002A. GEOCHEMICAL EVOLUTION OF LITHOSPHERIC MANTLE BENEATH SE SOUTH AUSTRALIA. ***CHEMICAL GEOLOGY*** **182, 663-695.**

FODEN J. D., ELBURG M. A., TURNER S. P., SANDIFORD M., O'CALLAGHAN J. & MITCHELL S. 2002B. GRANITE PRODUCTION IN THE DELAMERIAN OROGEN, SOUTH AUSTRALIA. ***JOURNAL OF THE GEOLOGICAL SOCIETY*** **159, 557-575.**

FODEN J. D., ELBURG M. A., TURNER S. P., SANDIFORD M., O C. J. & MITCHELL S. 2002C. GRANITE PRODUCTION IN THE DELAMERIAN OROGEN, SOUTH AUSTRALIA. ***JOURNAL OF THE GEOLOGICAL SOCIETY OF LONDON*** **159 PART 5, 557-575.**

FODEN J. D., TURNER S. P. & MORRISON R. S. 1990. TECTONIC IMPLICATIONS OF DELAMERIAN MAGMATISM IN SOUTH AUSTRALIA AND WESTERN VICTORIA. ***JAGO J B*** **16, 465-482.**

FOSTER D. A. & GRAY D. R. 2000. EVOLUTION AND STRUCTURE OF THE LACHLAN FOLD BELT (OROGEN) OF EASTERN AUSTRALIA. ***ANNUAL REVIEW OF EARTH AND PLANETARY SCIENCES*** **28, 47-80.**

GLEN R. 2005. THE TASMANIDES OF EASTERN AUSTRALIA. ***GEOLOGICAL SOCIETY, LONDON, SPECIAL PUBLICATIONS*** **246, 23-96.**

GRAHAM S., PEARSON N., JACKSON S., GRIFFIN W. & O'REILLY S. 2004. TRACING CU AND FE FROM SOURCE TO PORPHYRY: IN SITU DETERMINATION OF CU AND FE ISOTOPE RATIOS IN SULFIDES FROM THE GRASBERG CU–AU DEPOSIT. ***CHEMICAL GEOLOGY*** **207, 147-169.**

GRIESSMANN M. 2011. GOLD MINERALISATION IN THE ADELAIDE FOLD BELT.

GUM J. 1998. THE SEDIMENTOLOGY, SEQUENCE STRATIGRAPHY AND MINERALISATION OF THE SILVERTON SUBGROUP, SOUTH AUSTRALIA. UNIVERSITY OF SOUTH AUSTRALIA (UNPUBL.).

HAINES P., JAGO J. & GUM J. 2001. TURBIDITE DEPOSITION IN THE CAMBRIAN KANMANTOO GROUP, SOUTH AUSTRALIA. ***AUSTRALIAN JOURNAL OF EARTH SCIENCES*** **48, 465-478.**

HAINES P. W., TURNER S., FODEN J. D. & JAGO J. B. 2009. ISOTOPIC AND GEOCHEMICAL CHARACTERISATION OF THE CAMBRIAN KANMANTOO GROUP, SOUTH AUSTRALIA: IMPLICATIONS FOR STRATIGRAPHY AND PROVENANCE. ***AUSTRALIAN JOURNAL OF EARTH SCIENCES*** **56, 1095-1110.**

HOEFS J. 2009. ***STABLE ISOTOPE GEOCHEMISTRY*****. SPRINGER.**

HORN I., VON BLANCKENBURG F., SCHOENBERG R., STEINHOEFEL G. & MARKL G. 2006. IN SITU IRON ISOTOPE RATIO DETERMINATION USING UV-FEMTOSECOND LASER ABLATION WITH APPLICATION TO HYDROTHERMAL ORE FORMATION PROCESSES. ***GEOCHIMICA ET COSMOCHIMICA ACTA*** **70, 3677-3688.**

INDUSTRIES D. O. P. & AUSTRALIA S. 2007. KANMANTOO MINERALISATION.

IRELAND T., FLÖTTMANN T., FANNING C., GIBSON G. & PREISS W. 1998. DEVELOPMENT OF THE EARLY PALEOZOIC PACIFIC MARGIN OF GONDWANA FROM DETRITAL-ZIRCON AGES ACROSS THE DELAMERIAN OROGEN. ***GEOLOGY*** **26, 243-246.**

JAGO J. B. G. J. C., BURTT A. C. & HAINES P. W. 2003. STRATIGRAPHY OF THE KANMANTOO GROUP: A CRITICAL ELEMENT OF THE ADELAIDE FOLD BELT AND THE PALAEO-PACIFIC PLATE MARGIN, EASTERN GONDWANA. ***AUSTRALIAN JOURNAL OF EARTH SCIENCES.*** **50, 343-363.**

KITA N. T., HUBERTY J. M., KOZDON R., BEARD B. L. & VALLEY J. W. 2011. HIGH-PRECISION SIMS OXYGEN, SULFUR AND IRON STABLE ISOTOPE ANALYSES OF GEOLOGICAL MATERIALS: ACCURACY, SURFACE TOPOGRAPHY AND CRYSTAL ORIENTATION. ***SURFACE AND INTERFACE ANALYSIS*** **43, 427-431.**

KOIDE H. & BHATTACHARJI S. 1975. FORMATION OF FRACTURES AROUND MAGMATIC INTRUSIONS AND THEIR ROLE IN ORE LOCALIZATION. ***ECONOMIC GEOLOGY*** **70, 781-799.**

LAMBERT I. B., DONNELLY T., ETMINAN H. & ROWLANDS N. 1984. GENESIS OF LATE PROTEROZOIC COPPER MINERALIZATION, COPPER CLAIM, SOUTH AUSTRALIA. ***ECONOMIC GEOLOGY*** **79, 461-475.**

OHMOTO H. 1972. SYSTEMATICS OF SULFUR AND CARBON ISOTOPES IN HYDROTHERMAL ORE DEPOSITS. ***ECONOMIC GEOLOGY*** **67, 551-578.**

OHMOTO H. & LASAGA A. C. 1982. KINETICS OF REACTIONS BETWEEN AQUEOUS SULFATES AND SULFIDES IN HYDROTHERMAL SYSTEMS. ***GEOCHIMICA ET COSMOCHIMICA ACTA*** **46, 1727-1745.**

OHMOTO H. & RYE R. 0.(1979) ISOTOPES OF SULFUR AND CARBON. ***GEOCHEMISTRY OF HYDROTHERMAL ORE DEPOSITS*****, 509-567.**

OLIVER N., DIPPLE G., CARTWRIGHT I. & SCHILLER J. 1998. FLUID FLOW AND METASOMATISM IN THE GENESIS OF THE AMPHIBOLITES-FACIES, PELITE-HOSTED KANMANTOO COPPER DEPOSIT, SOUTH AUSTRALIA. ***AMERICAN JOURNAL OF SCIENCE*** **298, 181-218.**

PARKER A. 1986. TECTONIC DEVELOPMENT AND METALLOGENY OF THE KANMANTOO TROUGH IN SOUTH AUSTRALIA. ***ORE GEOLOGY REVIEWS*** **1, 203-212.**

PAYTAN A., KASTNER M., CAMPBELL D. & THIEMENS M. H. 1998. SULFUR ISOTOPIC COMPOSITION OF CENOZOIC SEAWATER SULFATE. ***SCIENCE*** **282, 1459-1462.**

POTTS G. J. & REDDY S. M. 1999. CONSTRUCTION AND SYSTEMATIC ASSESSMENT OF RELATIVE DEFORMATION HISTORIES. ***JOURNAL OF STRUCTURAL GEOLOGY*** **21, 1245-1253.**

POTTS G. J. & REDDY S. M. 2000. APPLICATION OF YOUNGING TABLES TO THE CONSTRUCTION OF RELATIVE DEFORMATION HISTORIES—1: FRACTURE SYSTEMS. *JOURNAL OF STRUCTURAL GEOLOGY* 22, 1473-1490.

REDDY S. M. & POTTS G. J. 1999. CONSTRAINING ABSOLUTE DEFORMATION AGES: THE RELATIONSHIP BETWEEN DEFORMATION MECHANISMS AND ISOTOPE SYSTEMATICS. *JOURNAL OF STRUCTURAL GEOLOGY* 21, 1255-1265.

RICHARDS J. 2003. TECTONO-MAGMATIC PRECURSORS FOR PORPHYRY CU-(MO-AU) DEPOSIT FORMATION. *ECONOMIC GEOLOGY* 98, 1515-1533.

RICHARDS J. P. 2009. POSTSUBDUCTION PORPHYRY CU-AU AND EPITHERMAL AU DEPOSITS: PRODUCTS OF REMELTING OF SUBDUCTION-MODIFIED LITHOSPHERE. *GEOLOGY* 37, 247-250.

RYE R. O. 2005. A REVIEW OF THE STABLE-ISOTOPE GEOCHEMISTRY OF SULFATE MINERALS IN SELECTED IGNEOUS ENVIRONMENTS AND RELATED HYDROTHERMAL SYSTEMS. *CHEMICAL GEOLOGY* 215, 5-36.

SANDIFORD M., FODEN J., ZHOU S. & TURNER S. 1992. GRANITE GENESIS AND THE MECHANICS OF CONVERGENT OROGENIC BELTS WITH APPLICATION TO THE SOUTHERN ADELAIDE FOLD BELT. *TRANSACTIONS OF THE ROYAL SOCIETY OF EDINBURGH: EARTH SCIENCES* 83, 83-93.

SANDIFORD M., FRASER G., ARNOLD J., FODEN J. & FARROW T. 1995. SOME CAUSES AND CONSEQUENCES OF HIGH-TEMPERATURE, LOW-PRESSURE METAMORPHISM IN THE EASTERN MT LOFTY RANGES, SOUTH AUSTRALIA. *IN:* OLIVER NICHOLAS H. S., CARTWRIGHT I. & RUBENACH MICHAEL J. EDS., *MID- TO LOWER-CRUSTAL METAMORPHISM AND FLUID-ROCK INTERACTION, WITH REFERENCE TO THE MT. ISA INLIER.*, VOL. 42; 3, PP 233-240, BLACKWELL, MELBOURNE, VICTORIA, AUSTRALIA.

SANDIFORD M., OLIVER R. L., MILLS K. J. & ALLEN R. V. 1990. A CORDIERITE-STAUROLITE-MUSCOVITE ASSOCIATION, EAST OF SPRINGTON, MT LOFTY RANGES; IMPLICATIONS FOR THE METAMORPHIC EVOLUTION OF THE KANMANTOO GROUP. *IN:* JAGO J. B. & MOORE P. S. EDS., *THE EVOLUTION OF A LATE PRECAMBRIAN-EARLY PALAEOZOIC RIFT COMPLEX; THE ADELAIDE GEOSYNCLINE.*, VOL. 16, PP 483-495, GEOLOGICAL SOCIETY OF AUSTRALIA, SYDNEY, N.S.W., AUSTRALIA.

SCHILLER J. C. 2000. STRUCTURAL GEOLOGY, METAMORPHISM AND ORIGIN OF THE KANMANTOO COPPER DEPOSIT, SOUTH AUSTRALIA. ADELAIDE UNIVERSITY, DEPARTMENT OF GEOLOGY AND GEOPHYSICS (UNPUBL.).

SECCOMBE P., SPRY P., BOTH R., JONES M. & SCHILLER J. 1985. BASE METAL MINERALIZATION IN THE KANMANTOO GROUP, SOUTH AUSTRALIA; A REGIONAL SULFUR ISOTOPE STUDY. *ECONOMIC GEOLOGY* 80, 1824-1841.

SILLITOE R. 1997. CHARACTERISTICS AND CONTROLS OF THE LARGEST PORPHYRY COPPER-GOLD AND EPITHERMAL GOLD DEPOSITS IN THE CIRCUM-PACIFIC REGION. *AUSTRALIAN JOURNAL OF EARTH SCIENCES* 44, 373-388.

SILLITOE R. H. & HEDENQUIST J. W. 2003. LINKAGES BETWEEN VOLCANOTECTONIC SETTINGS, ORE-FLUID COMPOSITIONS, AND EPITHERMAL PRECIOUS METAL DEPOSITS. *SPECIAL PUBLICATION-SOCIETY OF ECONOMIC GEOLOGISTS* 10, 315-343.

SKIRROW R. G., BASTRAKOV E. N., BAROVICH K., FRASER G. L., CREASER R. A., FANNING C. M., RAYMOND O. L. & DAVIDSON G. J. 2007. TIMING OF IRON OXIDE CU-AU-(U) HYDROTHERMAL ACTIVITY AND ND ISOTOPE CONSTRAINTS ON METAL SOURCES IN THE GAWLER CRATON, SOUTH AUSTRALIA. *ECONOMIC GEOLOGY* 102, 1441-1470.

SKWARNECKI M. & FITZPATRICK R. 2003. MOUNT TORRENS LEAD PROSPECT, SOUTH AUSTRALIA. *PROSPECTS* 183, 200.

STYRT M., BRACKMANN A., HOLLAND H., CLARK B., PISUTHA-ARNOND V., ELDRIDGE C. & OHMOTO H. 1981. THE MINERALOGY AND THE ISOTOPIC COMPOSITION OF SULFUR IN HYDROTHERMAL SULFIDE/SULFATE DEPOSITS ON THE EAST PACIFIC RISE, 21 N LATITUDE. *EARTH AND PLANETARY SCIENCE LETTERS* 53, 382-390.

TOTEFF S. 1977. THE GEOLOGY OF THE ADELAIDEAN-KANMANTOO GROUP SEQUENCES IN THE EASTERN MOUNT LOFTY RANGES.

TURNER S. & FODEN J. 1996. MAGMA MINGLING IN LATE-DELAMERIAN A-TYPE GRANITES AT MANNUM, SOUTH AUSTRALIA. *MINERALOGY AND PETROLOGY* 56, 147-169.

TURNER S., FODEN J. & MORRISON R. 1992. DERIVATION OF SOME A-TYPE MAGMAS BY FRACTIONATION OF BASALTIC MAGMA: AN EXAMPLE FROM THE PADTHAWAY RIDGE, SOUTH AUSTRALIA. ***LITHOS*** **28, 151-179.**

TURNER S., FODEN J., SANDIFORD M. & BRUCE D. 1993. SM-ND ISOTOPIC EVIDENCE FOR THE PROVENANCE OF SEDIMENTS FROM THE ADELAIDE FOLD BELT AND SOUTHEASTERN AUSTRALIA WITH IMPLICATIONS FOR EPISODIC CRUSTAL ADDITION. ***GEOCHIMICA ET COSMOCHIMICA ACTA*** **57, 1837-1856.**

TURNER S., KELLEY S., VANDENBERG A., FODEN J. D., SANDIFORD M. & FLÖTTMANN T. 1996. SOURCE OF THE LACHLAN FOLD BELT FLYSCH LINKED TO CONVECTIVE REMOVAL OF THE LITHOSPHERIC MANTLE AND RAPID EXHUMATION OF THE DELAMERIAN-ROSS FOLD BELT. ***GEOLOGY*** **24, 941-944.**

TURNER S., SANDIFORD M., FLÖTTMANN T. & FODEN J. 1994. RB/SR DATING OF DIFFERENTIATED CLEAVAGE FROM THE UPPER ADELAIDEAN METASEDIMENTS AT HALLETT COVE, SOUTHERN ADELAIDE FOLD BELT. ***JOURNAL OF STRUCTURAL GEOLOGY*** **16, 1233-1241.**

APPENDIX A: FULL METHODS

METHODS

Field work.

Field work was undertaken in the Spitfire Pit of the Kanmantoo copper mine, operated by Hillgrove Resources, located 55 kilometres south east of Adelaide in the eastern Mount Lofty Ranges. Field work was conducted in several stages to provide a structural analysis of the setting of the Kanmantoo copper deposit, focusing on the structural controls of mineralisation and alterations present. Analysis included collecting general observations of macro and micro structures, structural mapping, vein paragenesis and the relationships of these structural features to geochemical analysis.

Face Mapping

Detailed face mapping was undertaken on an exposed face in the Spitfire Pit. The face is situated on the 1190 RL and is 175 metres in length and incorporates known areas of

copper mineralisation as well as chlorite and iron alteration. The mapping was completed the 1 metre scale, with the use of a tape measure and compass clinometer. Marker numbers were sprayed on the wall every 5 metres and these numbers were surveyed by Hillgrove mine surveyors after the completion of mapping. This was done to allow entry into SURPAC mining software to later generate accurate 3D digital mapping with X, Y and Z co-ordinates in local mine grid.

The mapping focused on lithology and alteration as well as all structural features such as foliation, bedding, cleavage sets, faults, folds that were present. The mapping took special interest in S-C fabric and any veining, specifically quartz, sulphide or other, which was present along with any apparent cross cutting relationships to determine timing of veining in association to all other fabrics present along with any alteration that may accompany the veining.

Photographs were taken of the entire face, which were then stitched together to allow the face mapping to be overlain when completed. Photographs were also taken of features of interest as well as any significant structures or relationships that were discovered during mapping.

Vein Paragenesis and Timing

After face mapping was completed a specific study focusing on the styles of veining was undertaken. This involved measuring all veins that were discovered during

mapping along with recording their specific lithology, size and any deformation present. 65 veins were discovered and these were analysed with stereonets, using the *Georient* program, to investigate any trends and significant relationships of the veins to each other, and against other structural features such as bedding, faults and foliation.
A vein younging table was then completed (Potts et. al, 1999) to determine the order and timing of the veins present. This was completed by analysing the cross cutting relationships of the veins to each other to determine the order of vein paragenesis.

XRF Niton geochemical analysis

Geochemical analysis of the mapped 1190 RL bench was then undertaken by XRF handheld Niton. This was done in 2 stages:

1. Bulk Geochemistry

   2 lines of samples were taken 30cm intervals across the entire mapped face. These lines were 50cm apart with the lower line being the A sample, and the upper line being the B sample. A total of 896 samples were taken. These samples were 1 minute readings, running 4 filters for 15 seconds each. This reading length has been advised to be appropriate by the Niton handheld XRF manual as sufficient for each filter as errors are less than 40ppm after this reading time. This is considered appropriate for bulk geochemical sampling where ore zones are typically 10000ppm copper.
   Standards were run every 20 samples to allow consistent sampling and removal of any error and allow consistent sampling. These standards were created from grade control pulps that were collected during resource drilling of the deposit. These standards were assayed independently at two different labs and the pulps

were then made into pellet disks to enable a consistent method of sampling which is appropriate for the handheld XRF Niton gun. Before running each set of standards a pure silica standard was analysed to ensure the lens of the gun was clean from contaminants such as dust and dirt.

After sampling was completed the data were calibrated against the standards to remove any errors that occurred when sampling. This was done in Microsoft Excel and is included in the appendix of this paper.

The results of this geochemical analysis were then compared spatially against the face mapping outlined above to investigate the structural controls on element distribution, specifically copper mineralisation.

2. Localised Geochemistry

After analysis of bulk geochemistry against face mapping, 5 areas that showed significant mineralisation or structural significance to mineralisation were selected for closer geochemical analysis. These areas are 1 square metre, and involved XRF Niton analysis on a 10 x 10 cm grid. This closer grid spacing was in order to obtain better resolution and accuracy with the Niton handheld XRF and give a more detailed geochemical analysis. Standards were again run in a similar manner outlined in bulk geochemistry. The grids were photographed, with the geochemical results overlain to allow analysis of micro structure and their relationship to element distribution.

Micro – analysis

THIN SECTION

From results gathered during field mapping and XRF Niton geochemical sampling samples were taken for thin section to allow micro analysis. 30 µm polished thin sections were prepared by Pontifex, and were carbon coated prior to micro-analysis. A Nikon petrographic microscope was used for petrographic studies and for imagery.

SULPHUR ISOTOPE ANALYSIS (SIMS)

The CAMECA IMS 1280 high resolution, multi-collector ion microprobe (CAMECA 2012), located at the Centre for Microscopy, Characterisation & Analysis (CMCA) at The University of Western Australia, was used to perform in situ sulphur isotope analysis ($^{34}S/^{33}S$) of chalcopyrite from the polished block samples.

Samples were prepared by cutting small (<5mm^2) portions of the polished ore blocks and mounting them in epoxy resin with Son Std. Three to four samples were used in each mount and the pyrite grain mounts were Au-coated (~50nm) before analysis was carried out.

The grains of Son standard which were cast in the centre of each sample mount were measured five times initially to account for instrument drift, and then in at least two

spots before and after every ~8-10 sample analyses. The standard deviations of the Son standard analyses are equal to ± 0.13%.

The method used had a total running time of three minutes and 15 seconds, with the acquisition time being two minutes and 53 seconds. A spot size was 10µm and impact energy of 20,000V was used, resulting in an average sample emission of ~0.73µA. Raw measured $^{34}S/^{32}S$ and $^{33}S/^{32}S$ ratios were converted to the delta notation of $\delta^{34}S$ and $\delta^{33}S$ respectively by normalising to Vienna Cañon Diablo Troilite values. **$(^{34}S/^{32}S)_{VCDT}$ = 0.044163 and $^{33}S/^{32}S_{VCDT}$ = 0.00015368** (Ding *et al.* 2001, Kita *et al.* 2011).

Drift correction was applied to collected data in Microsoft excel where regression was significant.

APPENDIX B: XRF CALIBRATIONS

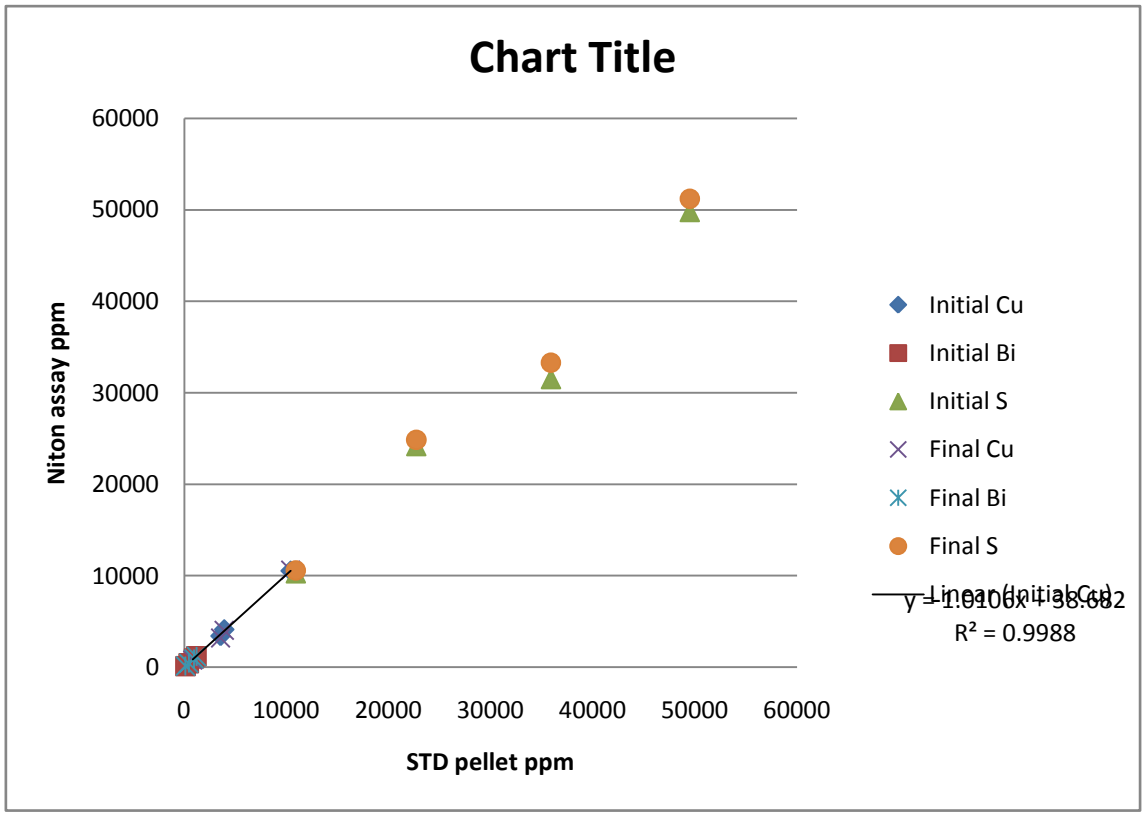

	StD No	Cu ppm	Cu Error	Bi	Bi Error	S ppm	S Error	Fe	Fe Error	Ag	Ag Error	Au	Au Error
initial	ST1	877.3	44.21	131.9	9.77	10288.13	302.63	109140.5	903.68	< LOD	11.46	< LOD	36.25
initial	ST2	3435.25	100	447.98	19.24	31508.01	566.82	157109.3	1324.02	< LOD	13.71	< LOD	43.7
initial	ST3	10554.17	188.16	962.47	27.97	49766.96	710.97	123544.3	1051.49	< LOD	12	< LOD	44.86
initial	ST4	4145.97	100.39	1209.57	29.82	24189.55	443.92	106312	900.57	< LOD	11.68	< LOD	42.82
	StD No	Cu ppm	Cu Error	Bi	Bi Error	S ppm	S Error	Fe	Fe Error	Ag	Ag Error	Au	Au Error
final	ST1	797.25	43.26	130.42	9.93	10576.57	309.45	108285	917.2	< LOD	10.04	< LOD	40.06
final	ST2	3195.75	98.51	433.22	19.37	33299.31	578.8	155145.1	1345.31	< LOD	13.51	< LOD	43.93
final	ST3	10622.4	186.34	917.91	26.89	51213.48	731.46	123573.3	1035.63	< LOD	11.82	< LOD	42.21
final	ST4	4058.07	101.46	1188.85	30.16	24843.54	468.13	105034.3	913.72	< LOD	10.61	< LOD	41.66

Pellet ID	Cu_ppm	Cu_pct	Ag_ppm	Bi_ppm	Bi_pct	S_pct	S_ppm
ST1	814	0.08	-5	113	0.0113	1.09	10900
ST2	3537	0.35	-5	437	0.0437	3.59	35900
ST3	10408	1.04	-5	946	0.0946	4.95	49500
ST4	3902	0.39	-5	1186	0.1186	2.27	22700
ST5	814	0.08	-5	113	0.0113	1.09	10900
ST6	3537	0.35	-5	437	0.0437	3.59	35900
ST7	10408	1.04	-5	946	0.0946	4.95	49500
ST8	3902	0.39	-5	1186	0.1186	2.27	22700

Initial				
Cu Slope	**Cu Intercept**	**r2**		
1.010555	38.68173735	0.999534626		38.68174
Bi Slope	**Bi Int**	**r2**		
1.005074	14.0778078	0.999955074		14.07781
S Slope	**S Int**	**r2**		
0.97514	-72.262719	0.988336922		72.26272
Final				
Cu Slope	**Cu Intercept**	**r2**		
1.031443	-143.569668	0.998874273		143.5697
Bi Slope	**Bi Int**	**r2**		
0.978643	11.41977657	0.999440123		11.41978
S Slope	**S Int**	**r2**		
1.010603	-82.2264038	0.991821034		82.2264

APPENDIX C: IOGAS TENARY PLOTS